

ISTANBUL TECHNICAL UNIVERSITY ★ GRADUATE SCHOOL OF SCIENCE
ENGINEERING AND TECHNOLOGY

**NUMERICAL INVESTIGATION OF AERODYNAMIC AND AEROACOUSTIC
PROPERTIES OF A SUPERSONIC JET**

M.Sc. THESIS

Ramiz Ömür İÇKE

Department of Mechanical Engineering

Heat-Fluid Programme

OCT 2015

ISTANBUL TECHNICAL UNIVERSITY ★ GRADUATE SCHOOL OF SCIENCE
ENGINEERING AND TECHNOLOGY

**NUMERICAL INVESTIGATION OF AERODYNAMIC AND AEROACOUSTIC
PROPERTIES OF A SUPERSONIC JET**

M.Sc. THESIS

Ramiz Ömür İÇKE
(503121124)

Department of Mechanical Engineering

Heat-Fluid Programme

Thesis Advisor: Prof. Dr. İ. Bedii ÖZDEMİR

OCT 2015

İSTANBUL TEKNİK ÜNİVERSİTESİ ★ FEN BİLİMLERİ ENSTİTÜSÜ

**SES ÜSTÜ BİR JETİN AERODİNAMİK VE AERO AKUSTİK
ÖZELLİKLERİNİN NUMERİK OLARAK İNCELENMESİ**

YÜKSEK LİSANS TEZİ

**Ramiz Ömür İÇKE
(503121124)**

Makina Mühendisliği Anabilim Dalı

Isı Akışkan Programı

Tez Danışmanı: Prof. Dr. İ. Bedii ÖZDEMİR

EKİM 2015

Ramiz Ömür İÇKE, a M.Sc. student of ITU Graduate School of Science Engineering and Technology student ID 503121124, successfully defended the thesis entitled “NUMERICAL INVESTIGATION OF AERODYNAMIC AND AEROACOUSTIC PROPERTIES OF A SUPERSONIC JET”, which he prepared after fulfilling the requirements specified in the associated legislations, before the jury whose signatures are below.

Thesis Advisor : **Prof. Dr. İ. Bedii ÖZDEMİR**
İstanbul Technical University

Jury Members : **Dr. Orhan ATABAY**
İstanbul Technical University

Assist. Prof. Dr. Özgür ERTUNÇ
Özyeğin University

Date of Submission : 02 Sep 2015
Date of Defense : 09 Oct 2015

To my family,

FOREWORD

This thesis is written as completion to the heat and fluid master program, at the Istanbul Technical University. The master programme focuses on behaviors of nature from fluid and heat mechanism point of view. The subject of this thesis is fluid based acoustic level evaluation by utilizing numerical method developed for supersonic jet flow. I have chosen to add computational aero acoustic to my professional skills, in line with the research field of the master.

All the effort put into this Master Assignment would not be enough, if I did not have the support of my loving family and friends around me. Therefore, I would like to thank my father, Opr. Dr. Uğur Mehmet İçke, my mother, Mahizer İçke and my sister, Melike İçke, for being strict when I needed it and their priceless advice and support they were always ready to give. And also, I would like to thanks my girlfriend, Yurdagül Çağlayan, who did not hesitate to help me with any difficulties I encountered. This support would not be complete without the helping hand of my supervisor from Ford Otosan, Dr. Cenk Dinç and my workmate. My friends made sure I had the necessary distraction during the process of research and always came up with handy ideas.

Since September 2014 I have been conducting research on the topic. I have experienced this period as very interesting and instructive. At the beginning I had little knowledge of acoustics and computational fluid dynamics. However, I have been able to achieve a result I am very satisfied with. I would like to thank my supervisor from the University, Prof. Dr. İ. Bedii Özdemir from Mechanical Engineering Department. His valuable insights and directions gave me needful guidance to complete the research and write this thesis. Moreover, I would like to thank Assoc. Prof. Dr. Mehmet Şahin for his greatful support from computational fluid dynamics perspective and Prof. Dr. Rüstem Arslan for his supportive approaches.

Thereby I would like to close one chapter of my life and open up a different one, hopefully as interesting and rewarding as the three years of studying at the Istanbul Technical University.

Oct 2015

Ramiz Ömür İÇKE
(Aeronautical and Astronautical
Engineer)

TABLE OF CONTENTS

	<u>Page</u>
FOREWORD	ix
TABLE OF CONTENTS	xi
ABBREVIATIONS	xiii
NOMENCLATURE	xv
LIST OF FIGURES	xvii
SUMMARY	xix
ÖZET	xxi
1. INTRODUCTION	25
1.1 Importance of Aero-Acoustics	25
1.2 Goal of The Thesis Project	27
2. COMPUTATIONAL FLUID DYNAMICS	29
2.1 Direct Numerical, Large Eddy and Detached Eddy Simulation	30
2.2 Linearized Euler Equation	31
2.2.1 Van-Leer flux splitting method	33
2.2.2 Roe method	34
2.2.3 Solution scheme AUSM+ (Advaction Upstream Splitting Method)	35
2.2.3.1 Boundary conditions	39
3. AEROACOUSTICS	41
3.1 Basics of Acoustics	41
3.1.1 Acoustic perception	41
3.1.2 Acoustic sources	41
3.2 Aeroacoustics Integral Methods	43
3.2.1 Lighthill's analogy	43
3.2.2 Ffowcs Williams-Hawkings equations	46
3.2.3 Kirchhoff method	48
3.3 Acoustic Mathematics	49
3.3.1 Green's theorem	49
3.3.2 Fourier transform	50
3.3.3 Nyquist criteria	52
3.3.4 Strouhal number	52
4. STUDY DESCRIPTION	53
4.1 Base Study	53
4.2 Model Setup and Solution Scheme	57
5. RESULTS	63
5.1 Aerodynamic Assessments	63
5.2 Acoustic Assessments	68
6. CONCLUSIONS AND RECOMMENDATIONS	73
REFERENCES	75
APPENDICES	77
CURRICULUM VITAE	79

ABBREVIATIONS

CAA	: Computational Aero Acoustic
CFD	: Computational Fluid Dynamics
DES	: Dettached Eddy Simulation
DNS	: Direct Numeric Solution
LES	: Large Eddy Simulation
LEE	: Linearized Euler Equation
FWH	: Ffowcs Williams Hawking Method
FFT	: Fast Fourier Transform

NOMENCLATURE

a_0	: Initial sound velocity
$a_{1/2}$: Sound velocity at target point
a_L	: Sound velocity left hand side of target point
a_R	: Sound velocity right hand side of target point
A_E	: Area of grid element
c_0	: initial sound velocity
c_p	: Specific Heat Coefficient
c_v	: Specific Heat Coefficient
d_{ij}	: direction of grid edge
D	: Tube diameter
D_{NE}	: Nozzle exit diameter
e	: Unit energy term
e_0	: Initial unit energy term
e_t	: Unit energy term at t
E	: Total energy term
E_e	: Energy flux in LES
E_v	: Viscous term of energy
E_∞	: Infinite energy term
F_e	: Energy flux
F_v	: Viscous term
f	: Inviscid flux
f_a	: Actual frequency
f_c	: The highest frequency in the signal
f_s	: Sampling frequency
f_v	: Shedding frequency
G	: Green function
I	: Intensity of sound
H	: Enthalpy
K_p	: Pressure kappa
K_u	: Pressure kappa
$\dot{m}_{1/2}$: Mass flux at target point
M	: Mach number
M_0	: Initial mach number
$M_{L/R}$: Approach mach number
M_L	: LHS mach number
M_R	: RHS mach number
n	: Normal vector
n_l	: Normal vector of edge of grid
N	: Number of frequency component
Q	: State vector
Q_∞	: State vector at inflow
Q_L	: State vector at LHS
Q_R	: State vector at RHS
q_j	: Heat Flux
P	: Pressure
P_0	: Mean value of static pressure

p	: Pressure
p_L	: LHS Pressure
p_R	: RHS Pressure
p_∞	: Inflow Pressure
R	: Specific heat ratio
Re	: Reynolds number
St	: Strouhal number
S_l	: Parpendicular vector of normal vector of grid edge
t	: Time
T	: Temperature
T_{ij}	: Sound source tensor
\hat{T}	: Mean temperature
U	: Free flow velocity
U_j	: Free flow velocity at any x_j direction
u	: Velocity at x direction
$u_{L/R}$: Velocity at x direction interms of variable approach point
u_L	: Velocity at x direction for LHS
u_R	: Velocity at x direction for RHS
u_∞	: Velocity at x direction for freestream
V	: Gap flow velocity
v	: Velocity at y direction
v_∞	: Velocity at x direction for freestream
W_N	: Periodic fourier function
α	: Alfa
β	: Beta
γ	: Gamma
δ	: Kronecker number
δ_{ij}	: Kronecker number for variable axis
μ	: Dynamic viscosity
σ	: Prandtl number
ρ	: Density
ρ_0	: Initial Density
$\rho_{1/2}$: Density for target point
ρ_L	: Density for LHS
ρ_R	: Density for RHS
ρ_∞	: Density for freestream
τ_{ij}	: Stress tensor
φ	: Scallar field

LIST OF FIGURES

	<u>Page</u>
Figure 1.1 : Aircraft noise and public life	25
Figure 1.2 : Generated noise from automotive cooling fan	26
Figure 1.3 : Jet nozzle noise generated from turbofan engine	26
Figure 2.1 : Small infinitesimally element.....	29
Figure 2.2 : Approaching to point	34
Figure 2.3 : A sample grid structure and notation.....	38
Figure 3.1 : Theoretical directivity patterns for far-field sound pressure levels radiated from (a) monopole, (b) dipole, (c) lateral quadrupole and (d) longitudinal quadrupoles sound sources (Daniel A. Russell, 1999).....	42
Figure 4.1 : Small hot jet acoustic rig (SHJAR) (Bridges, 2012)	53
Figure 4.2 : NA2Z convergent nozzle.....	54
Figure 4.3 : Dimensions of nozzle	54
Figure 4.4 : Notation of microphones location angles	55
Figure 4.5 : Result of NASA test in terms of frequency vs dB.....	56
Figure 4.6 : Reference simulation result for mesh resolution effect.....	56
Figure 4.7 : Generation of 2D section.....	57
Figure 4.8 : Boundary conditions of domain	58
Figure 4.9 : Angles of quad element	58
Figure 4.10 : Grid structure.....	59
Figure 4.11 : Neighbouring pseudo code	59
Figure 4.12 : Main program pseudo code	60
Figure 5.1 : Refined solution domain (2nd assessment)	63
Figure 5.2 : Refined mesh resolution (2nd assessment).....	64
Figure 5.3 : Pressure values vs time from centreline points	64
Figure 5.4 : Velocity values vs time from centreline points	65
Figure 5.5 : Pressure distribution of domain at time equals to 0.48300	65
Figure 5.6 : Pressure distribution of domain at time equals to 0.4830 near to nozzle exit	66
Figure 5.7 : Overexpanded jet characteristics	66
Figure 5.8 : Density distribution of domain at time equals to 0.4830 near to nozzle exit	67
Figure 5.9 : Velocity distribution of domain at time equals to 0.4830 near to nozzle exit	67
Figure 5.10 : Benchmark study for pressure values at centerline $t=0.4$	68
Figure 5.11 : Acoustic pressure fluctuation field (Pressure RMS) (0.4s-0.8s)	68
Figure 5.12 : Microphone locations based on reference	69
Figure 5.13 : Pressure perturbation of microphone points.....	70
Figure 5.14 : Acoustic magnitude response vs frequency in octave band.....	70
Figure 5.15 : Jet noise contributions	71
Figure A.0.1 : Phases vs frequency	77

Figure A.0.2 : Density distribution on domain for $t=0.82550$	77
--	----

NUMERICAL INVESTIGATION OF AERODYNAMIC AND AEROACOUSTIC PROPERTIES OF A SUPERSONIC JET

SUMMARY

In many industrial applications, noise is an important point in human health, noise and social order. And having the appropriate frequency and noise as low as possible is desirable extent. Our environmental noise sources vary considerably. Traffic, industry, train, plane, is the environmental impact of construction noise reasons and so on. The resulting noise source may be due to different reasons. For example, friction between materials, explosions, interaction between air and solid can be given.

Nowadays, the lower noise level is required for vehicles such as car, aircraft and trains. Because of this situation it is mentioned by a number of specific criteria the commission. In addition, in terms of marketing it is an important component to vehicle comfort. Therefore, a lot of evaluations in the aerospace and automotive company to experiment on noise and writing articles, and, they're developing theories and making progress.

In the aviation industry, one of the major focus is sources of noise radiated from the engine nozzle. Lots of examinations and experiments were conducted in this scope. The nozzle exit creating pressure fluctuation as complex is a highly effective sound source location and this case for both the supersonic nozzle and subsonic nozzle is available. In the thesis scope, the noise level at the outlet of the supersonic jet nozzle base sound has been investigated by utilizing numerical methods.

In the first part of the thesis, a wide range of assessment of fluid mechanics and computational fluid dynamics methods has been mentioned. Here, how to evaluate the events of flow and how it can be modeled numerically are mainly focused on. Such as flow characteristics, solutions and approaches, important technical informations are given in the first chapter. Here, the Navier-Stokes equations and solving techniques are shown briefly such as Direct Numeric Simulation (DNS), Large Eddy Simulation (LES) and Detached Eddy Simulation (DES) methods. In addition, using Linearized Euler Equation (LEE), the solution of Euler's equation is shown. In this section, technical solutions that are available for LEE equations used for this thesis was examined. The most effective method, AUSM, are discussed in a comprehensive manner. In this thesis, the described model is solved using LEE-AUSM method.

In the second part, general concepts related to acoustic shown. Accordingly, technical details have been provided. In addition, acoustic analogies used in the literature is mentioned in this section. To name the main acoustic assessment methods, Lighthill analogy, Curle analogy, Ffowcs William-Hawking (FW-H) method and Kirchhoff method can be shown. the scope of the thesis, using Lighthill's method, total amount of noise has been computed from the light of LEE-AUSM output. The differences between methods, disadvantages and advantages of the methods are demonstrated in this section.

In the third section, main problem description and the details are located. Problems in other words discussed the issue is investigation of the use of a supersonic nozzle of the characters in the tests conducted by the National Aeronautics and Space Institute (NASA). Investigation of NASA's test of nozzle includes frequency, decibel scale and test conditions.

In the fourth chapter of the thesis, details of the modeling, coding structures assumptions and results are located. Network modeling details, the compliance with the CFD and the coding optimization can be found. The results fully belonging to code builder who is author of thesis study are discussed here. As a result of the simulation, flow diagrams, and graphs related to noise gradients are available.

In the last part of the thesis, NASA's results and code results obtained from numerical study are compared. Furthermore, using same condition, CFD applications used in industry benchmark study has been compiled in order to make validation of work. Moreover, compared numerical results and flow diagrams have been shown.

The scope of the results of obtained result, neglecting viscous flow and turbulence model approaches can be utilized for this type of supersonic flow in terms of shockband and frequencies analysis. Accordingly, correlation of the determined model shows similar idea. Same application can be applied to different model examination. From the assessments, shockband noise dominant or dependent results have been demonstrated.

SES ÜSTÜ BİR JETİN AERODİNAMİK VE AERO AKUSTİK ÖZELLİKLERİNİN NUMERİK OLARAK İNCELENMESİ

ÖZET

Birçok endüstriyel uygulamada, toplumsal düzende ve insan sağlığında gürültü önemli bir yer teşkil etmektedir. Gürültünün uygun frekansda ve olabildiğince düşük ölçüde olması arzulanmaktadır. Çevremizde gürültü kaynakları oldukça çeşitlilik göstermektedir. Trafik, sanayii, tren, uçak, inşaat vb nedenlerle gürültü çevreye etki etmektedir. Oluşan gürültü kaynağı farklı sebeplerden kaynaklanabilir. Örneğin malzemeler arası sürtünme, patlama, hava ile katının etkileşimi vb faktörler olabilir.

Günümüzde kullandığımız otomobil, uçak ve tren gibi taşıtlar için gürültü seviyesi yine minimal düzeyde istenmektedir. Bu durumdan ötürü birçok komisyon tarafından belirli kriterler konulmuştur. Buna ek olarak pazarlama açısından da gürültü taşıtlar için önemli bir konfor bileşeni durumundadır. Bu nedenden ötürü bir çok havacılık ve otomotiv firması gürültü üzerine deneyler yapmakta, makaleler yazmakta, teoriler üretmekte ve geliştirmeler yapmaktadırlar.

Havacılık endüstrisinde ise önemli odaklardan biri motor lülesindeki gürültü kaynağıdır. Bunu incelemek için bir çok inceleme ve deney gerçekleştirilmiştir. Lüle çıkışındaki gürültü basınç çalkantıları yaratması dolayısıyla oldukça etkili bir ses kaynağı konumundadır ve bu durum hem ses üstü lülelerde hem de ses altı lülelerde mevcuttur. Bu tez kapsamında ses üstü bir lülenin çıkış kısmındaki gürültü düzeyi sayısal yöntemler kullanılacak incelenecektir.

Tezin ilk bölümünde akışkanlar mekaniği ve hesaplamalı akışkanlar dinamiği metodları ile ilgili geniş bir değerlendirme mevcuttur. Burada temel olarak akış olaylarının nasıl değerlendirildiği ve bunun sayısal olarak nasıl modellenebileceği üzerinde durulmaktadır. Akış karakterleri, çözüm teknik ve yaklaşımlar ilk bölümde verilen önemli bilgiler arasındadır. Burada Direct Numeric Simulation (DNS), Large Eddy Simulation (LES) ve Detached Eddy Simulation (DES) gibi Navier-Stokes denklemini çözen teknikler kısaca gösterilmektedir. Buna ek olarak Linearized Euler Equation (LEE) kullanarak Euler denklemlerinin çözümü gösterilmektedir. Tez kapsamında LEE kullanıldığı için LEE denklemleri için mevcut olan çözüm teknikleri bu bölümde incelenmiştir. Burada en efektif olan AUSM metodu üzerinde kapsamlı bir şekilde durulmaktadır. Tez kapsamında LEE-AUSM metodu kullanılarak kontrol hacmindeki model çözülmektedir.

İkinci bölümde ise akustik ile ilgili genel geçer kavramlar gösterilmiştir. Bu kavrama dair teknik detay sağlanmıştır. Buna ek olarak literatürde kullanılan akustik analogiler yine bu bölümde bahsedilmektedir. Başlıca akustik değerlendirme yöntemlerini saymak gerekirse, bunlar Lighthill analogisi, Curle analogisi, Ffowcs William-Hawking (FW-H) metodu ve Kirchhof metodu gösterilebilir. Tez kapsamında LEE-AUSM methodunun elde ettiği çıktıların ışığında bu metodlardan Lighthill metodu kullanılarak toplam gürültü miktarı bulunmaya çalışılacaktır. Lighthill analogisi endüstride ve akademik literatürde en çok kullanılan yöntemlerden biridir. Lighthill metodu FLUENT, STAR-CCM vb bir çok ticari hesaplamalı akışkanlar programı tarafından kullanılmaktadır. Bu metod kapsamında yansıtıcı yüzey diğer bi deyişle

sesin yansıdığı durumları kullanmak doğru bir yaklaşım olmaz. Bu handikapı çözebilmek için FW-H ve Kirchhof yöntemi kullanılabilir. Tez kapsamında bu yöntemlere derinlikle bahsedilmemiş olup bu yöntemler arası farklar ,dezavantajlar ve avantajlar da yer almaktadır.

Ayrıca bölümün son kısmında akustik data elde edilışinde kullanılan temel matematiksel kuramlar incelenmiştir. Akustik yöntemde kullanılan matematiksel denklem olan green teoremi detaylı bir şekilde incelenmiştir. Buna ek olarak, çalkantının zamana göre dağılımı ses şiddetinin frekans ortamındaki dağılımının elde edilmesini sağlayan fourier transferinden bahsedilmiştir. Bunun hangi temellere dayandığı ve de nasıl elde edildiği yine bu kısımda gösterilmiştir. Son olarak, data kalitesini yani doğru örnekleme sağlayabilmek için önemli bir parametre olan Nyquist kriteri incelenmiştir. Proje kapsamında 100kHz lik daha toplama 50kHzlik data örnekleme mevcuttur. Bu Nyquist yaklaşımı kullanılarak elde edilmiştir.

Üçüncü bölümde ise, üzerinde durulan problemin detayları yer almaktadır. Problem diğer bir deyişle ele alınan durum Ulusal Havacılık ve Uzay Enstitüsü (NASA) nün gerçekleştirdiği testlerde kullandığı bir lülenin ses üstü durumdaki karakterinin incelenmesidir. NASA testi yapılmış olan lülenin frekans ve desibel ölçeğinin incelenmesi ve test koşulları yer almaktadır. Test koşullarının ne şekilde gerçekleştirildiği ve ölçümün ne şekilde yapıldığı gösterilmektedir. Testde kullanılan mikrofon setinin ses ölçümünde nasıl yerleştirildiği ve hata oranları da yine bu bölümde özetlenmektedir.

Tezin dördüncü bölümünde ise modellemenin detayları, kodlama yapısı, varsayımlar ve sonuçlar yer almaktadır. Burada yapılan ağ modellemesinin detayları, CFD ile uygunluğu, kodlama ile ilgili optimizasyonlar bulunabilir. Burada tezde çalışılan konu ile ilgili tamamen tez sahibine ait olan kod yapısının sonuçları irdelenmektedir. Simulasyon sonucunda akış diagramları, gradyenler ve gürültü ile ilgili grafikler mevcuttur. Şok dalgalarının belirgin lokasyonları, şok dalgalarının yayılım durumu yine bu bölümde gösterilmiştir.

Tezin son kısmında ise, NASA nın elde ettiği testler ile yazılan kod sonucunda elde edilmiş sayısal sonuçlar karşılaştırılmıştır. Buna ek olarak yine bu kısımda benchmark çalışması yapmak amacıyla endüstride kullanılan CFD uygulamalarında da aynı durum modellenmiştir. Burada sayısal sonuçlar ve akış diagramları karşılaştırılmıştır.

Sonuç olarak elde edilen sonuçlar kapsamında, geliştirilen kod şeması sayesinde, sıkıştırılabilir akışdaki akış çalkantıları basınç ve yoğunluk anlamında belirgin bir şekilde tespit edilebilmektedir. Lüle çıkışındaki akış karakteristiği sıkıştırılabilir akışkanlar presibine tamamen uygun olup şok baklavaları olarak adlandırdığımız yapılar oluşmaktadır. Bu yapılar içinde normal ve eğik şoklar sayesinde anlık olarak basınç ve yoğunluk değerleri değişmektedir. Özellikle lüle çıkışındaki eğik ve normal şok yapıları olması gerektiği oluşmuştur. Yüksek ve ani basınç ve yoğunluk farklılıkları bu yapıları gösteren en önemli parametrelerdir. Dolayısıyla, yüksek doğrulukla bulunan şok yapıları akustik hesaplamaların doğruluğunu önemli ölçüde artırmıştır.

Değişen basınç gradyenleri “broadband noise” dediğimiz yapıların kaynağını oluşturmaktadır. Bu tarz ses üstü akışlarda shockbandını ve frekansları doğru almak koşulu ile viskoz akış ve turbulence modeli yaklaşımları ihmal edilerek gerçek hayattan elde edilmiş sonuç ile belirgin bir sonuç farkı bulunmaktadır. Ancak şok yapısının doğru bir şekilde oluşturulması NASA test lerinde bazı frekanslarda uygunluk göstermiştir.

Gelecek çalışma kapsamında kodun içersine turbulans ve viskoz terim ler de eklenerek istenen en doğru akış ve acoustic karateristiği elde edilecektir. Bu çalışma kapsamında mevcut akış karakteristiği yeterli görülüp hangi kaynağın hidrolik çalkantıdan geldiği tespit edilmiştir.

Çalışma akustik kaynağın nasıl ayrıklaştığı hakkında uygun bir deneyim ve bilgi içermektedir. Diğer bir deyişle turbulans kaynaklı, hidrodinamik çalkantı kaynaklı veya şok kaynaklı akustik değerleri gösterir. Tez kapsamında şok kaynaklı durum için değerlendirme yapılmıştır.

Proje kapsamında geliştirilen kod farklı domain veya geometriler için tamamen uyumludur. Burada yapılan kod ile bir çok farklı model incelenebilir. Farklı problemlerde fiziksel durumlar değerlendirilebilir. Vizkoz terimlerin eklenmesi ile “shear noise” olarak adlandırdığımız duvara yakın bölgedeki çalkantıları bulmada yardımcı olacaktır. Doğal olarak buna turbulence terimleri de eklenmelidir doğrulu artırabilmek için. Bu sayede “mixing noise” ve “screech tone” adını verdiğimiz ses frekansları yakalanabilir.

1. INTRODUCTION

1.1 Importance of Aero-Acoustics

Acoustics have become one of the most important parameters for the design process in aerospace, automotive, naval and defense industries. There are two kinds of acoustic source, including fluid based and material based. In literature, fluid based acoustics are called aero-acoustics. Automobile a-pillar wind noise, aircraft winglet noise, aircraft engine jet noise, fan noise, etc. can be given for aero-acoustic examples. To reduce generated noise, many studies continued by physical tests and numerical methods are performed. Physical testing represents real situation and correlation error is too small. However, it's too hard to perform due to high expenses, safety risks and rig complexities. In this scope, numerical approaches have become the feasible point. Increasing computer capacities and abilities have made numeric simulation capable and affordable for aero-acoustic researches. Numerical aero-acoustic researches have been brought together under the same roof of Computational Aero Acoustic (CAA).



Figure 1.1 : Aircraft noise and public life

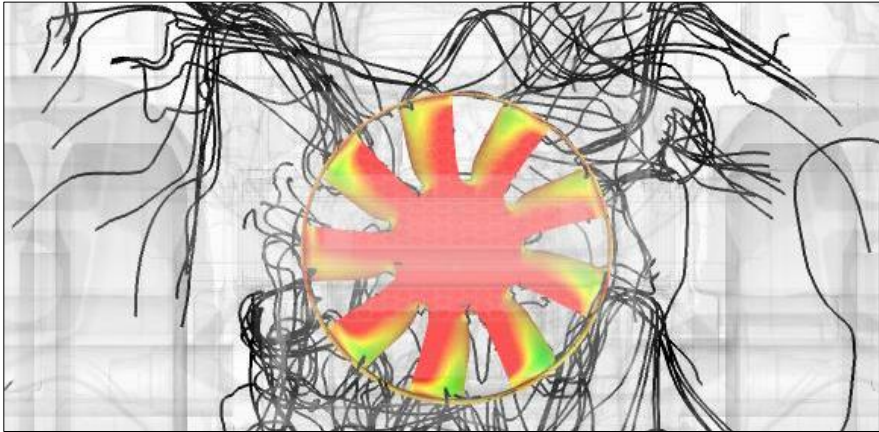


Figure 1.2 : Generated noise from automotive cooling fan



Figure 1.3 : Jet nozzle noise generated from turbofan engine

Computational aero-acoustic used for prediction of sound level works couple with Computational Fluid Dynamics (CFD). CAA predicts sound sources and propagation of the sound generation. To capture sound generation and radiation, CAA has high order accurate systems such as from 4th to 6th order as different from CFD which uses 2nd order approaches. There are too many applications in literature for CAA schemes and solver techniques. However, this discretization totally depends on the CFD method used as coupled. For instance, Reynolds Averaged Navier-Stokes (RANS), Unsteady Reynolds Averaged Navier-Stokes (URANS), Direct Numerical

Simulation (DNS), Large Eddy Simulation (LES), Detached Eddy Simulation (DES) etc. determines characteristic of the solution and then CAA methods computes sound related items. And, the CAA method selection comes from selected CFD method properties.

1.2 Goal of The Thesis Project

The goal of this thesis project is developing a method for predicting the sound produced by supersonic rectangular jet by Computational Fluid Dynamics (CFD) and Computational Aero Acoustic (CAA) in two-dimensional. Developed method has been modelled in-house code performed at MATLAB and correlation study has been performed with NASA's physical test that is already done. And utilized Acoustic Analogy originally based on Lighthill and Ffowcs Williams - Hawking studies. In the project, correlation study and algorithms usage has been figured in detail.

2. COMPUTATIONAL FLUID DYNAMICS

Computational Fluid Dynamics (CFD) is introduced as numerical calculation of domain relied on problem description. For example, to represent turbulence structure, it can be investigated in two sections that are laminar and turbulent flow. The real life problem defined, as clearly can be convert to calculation domain in a proper way. Flow description should have some assumption to solve problem. For instance, in nature medium, airflow is always compressible form but in numerical approach, flow below than 0.3 Mach number is assumed as incompressible flow. In this scope, main concern of this study can be clarified from numerical approach. Before clarification, some of the CFD methods were introduced as below.

In this project, whole CFD application depends on Navier-Stokes equations. Navier-Stokes equation is probably most widespread theoretical equation in fluid dynamics. It was derived from applying Newton's second law to fluid-flow momentum equation by Claude-Louis Navier and George Gabriel Stokes.

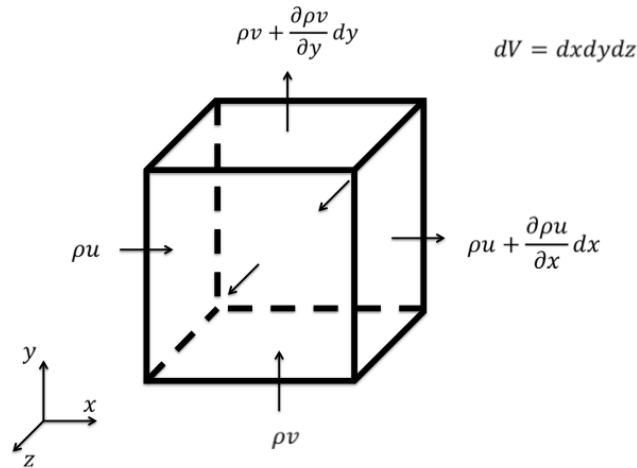


Figure 2.1 :Small infinitesimally element

Navier-Stokes equation (NS) is obtained using infinitesimally small element shown on above figure. Divergence at interval element supports whole problem domain to calculate overall equation for a sample control volume. From this point, first of all, continuity equation is derived (White, 2006),

$$\frac{\partial \rho}{\partial t} + \frac{\partial}{\partial x_j}(\rho v_j) = 0 \quad (2.1)$$

And momentum equation,

$$\frac{\partial}{\partial t}(\rho v_i) + \frac{\partial}{\partial x_j}[\rho v_i v_j + p \delta_{ij} - \tau_{ji}] = 0 \quad (2.2)$$

Addition to these two equations, energy equivalent is also important governing equation if temperature gradient affects problem at a certain level. Energy equation is again obtained from small finite element input-output energy balance as below.

$$\frac{\partial}{\partial t}(\rho e_0) + \frac{\partial}{\partial x_j}[\rho v_j e_0 + v_j p + q_j - v_i \tau_{ij}] = 0 \quad (2.3)$$

From these two equations, flow behaviour is predicted if another additional equation or things, which must be represented, doesn't exist. Modelling industrial application via CFD method is the main concern of CFD tools. This challenge becomes CFD applications, codes, algorithms and equation faster day by day. A lot of example can be reached from literature for CFD methods. Some of the applications will be introduced in this report brief.

2.1 Direct Numerical, Large Eddy and Detached Eddy Simulation

At first, Direct Numerical Simulation (DNS) that has the highest accuracy in literature will be handled. However, for commercial application or large domain it's not useful because of computation time and memory restriction.

In DNS, Navier-Stokes equation is solved without any turbulence modelling pack, which derived from test-CFD correlation studies. Turbulence models help solution for solving Reynolds-stress part. But DNS calculation, each turbulence scale is computed directly from the smallest scale to the largest scale. These length scales can be divided into three categories.

As second, LES can be utilized for investigating requested model. Similarly, LES solves turbulence structure directly without any turbulence model pack. But, as different as DNS, large scales of turbulence eddies are solved. Using LES near to wall or small mesh size is not logical. Applying LES to domain needs additional

filtering mechanism and it's executed before overall computation. After that LES is executed and appropriate region is solved. When LES is compared with DES, it has lower cost and time efficiency. There are a lot of applications for LES such as unsteady free stream, jet flow, exhaust flow etc.

As third, DES application also can be used for unsteady Navier-Stokes problems. DES is kind of hybrid method combining LES and RANS method, which is derived from test result correlated pre-defined turbulent model. Model separated in two different zones as near wall and far field is computed two different approaches. At zones near to wall are calculated by RANS methodology and for far field, calculation is executed using standard LES schemes. In other words, DES utilizes the best side of two different applications and it can be applied to too many cases due high capable capacity for fluid problem.

In thesis scope, these modules have not been used. This section has mentioned complexity and CPU consumption of the modules. Instead of these modules, simpler and more effective methods have been focused in the next sections.

2.2 Linearized Euler Equation

In this section, Linearized Euler Equation has been introduced. Linearized Euler Equation (LEE) is a kind of computation method for fluid flow. Basically, Euler's equation represents inviscid flow, in other words, viscous terms in the flow phenomena are neglected. Correspondingly, turbulence terms are ignored in fluid flow. Applying this assumption to Navier-Stokes Equation, Euler's Equation is obtained. According to focus point in the investigated problem, LEE can become a very useful approach in order to reduce computation time and algorithm complexities. LEE based method used for compressible, unsteady and inviscid problems.

The Euler equations can be described in 1-D as,

$$\frac{\partial}{\partial t} \begin{bmatrix} \rho \\ \rho u \\ E \end{bmatrix} + \frac{\partial}{\partial x} \begin{bmatrix} \rho u \\ \rho u^2 + p \\ (E + p)u \end{bmatrix} = 0 \quad (2.4)$$

Here, ρ, u, p represent density, velocity and pressure correspondingly.

$$E = \rho e + \frac{1}{2} \rho u^2 \text{ and } e = c_v T \quad (2.5)$$

If variable transformation is applied, the equation becomes,

$$\frac{\partial Q}{\partial t} + \frac{\partial f}{\partial x} = 0 \quad (2.6)$$

Q is state vector and f is inviscid flux. Using linearization, this equation converts to,

$$\frac{\partial Q}{\partial t} + \frac{\partial f}{\partial Q} \frac{\partial \varphi}{\partial x} = 0 \quad (2.7)$$

$$\frac{\partial f}{\partial Q} = [A] \rightarrow \text{Jacobian Matrix} \quad (2.8)$$

Then it becomes,

$$\frac{\partial Q}{\partial t} + [A] \frac{\partial Q}{\partial x} = 0 \quad (2.9)$$

This equation is called quasi-linear form of 1-D Euler Equation.

The Euler equations governing unsteady compressible inviscid flows can be expressed in 2D conservative form as:

$$\frac{\partial Q}{\partial t} + \frac{\partial F_1}{\partial x} + \frac{\partial F_2}{\partial y} = 0 \quad (2.10)$$

Where

$$Q = \begin{bmatrix} \rho \\ \rho u \\ \rho v \\ E \end{bmatrix} \quad F_1 = \begin{bmatrix} \rho u \\ \rho u^2 + p \\ \rho uv \\ u(E + p) \end{bmatrix} \quad F_2 = \begin{bmatrix} \rho v \\ \rho uv \\ \rho v^2 + p \\ v(E + p) \end{bmatrix} \quad (2.11)$$

The Euler equations are not complete without an equation of state. We choose an ideal gas for which

$$e_{int} = \frac{p}{\rho(\gamma - 1)} \quad (2.12)$$

And Quasi-linear form,

$$\frac{\partial Q}{\partial t} + [A] \frac{\partial Q}{\partial x} + [B] \frac{\partial Q}{\partial y} = 0 \quad (2.13)$$

After introducing linearized Euler's equation, solution methods can be described. The solution will be investigated from aero-acoustic character determination. Therefore, pressure fluctuation data are recorded at each time step. In literature, numerous methods having different advantages exist. The most important methods have been described as below.

2.2.1 Van-Leer flux splitting method

The Van Leer (1979) flux vector splitting is one of a large body of similar techniques. Since a general fluid flow contains wave speeds that are both positive and negative (so that eigenvalue information can pass both upstream and downstream), the basic idea behind all of these techniques is that the flux can be split into two components so that each may be properly discretized using relatively upwind stencils to maintain stability and accuracy. There are many possible ways to split the flux term by basing the splitting on the eigenvalue structure or some similar representation of the flow.

From Tannehill, Anderson, and Pletcher (1997), the particular Van Leer flux splitting sought to correct some problems found at sonic and stagnation points for an earlier splitting called Steger-Warming. The Van Leer splitting offers both zero and first order continuity through sonic and stagnation points, thus correcting this problem. This particular variation of flux splitting is based on Mach number splitting (Laney 1998). The Mach number for supersonic flow is simply the full scalar Mach number in the downwind direction, and zero in the upwind direction. For subsonic flow, the Mach number is slightly more complex.

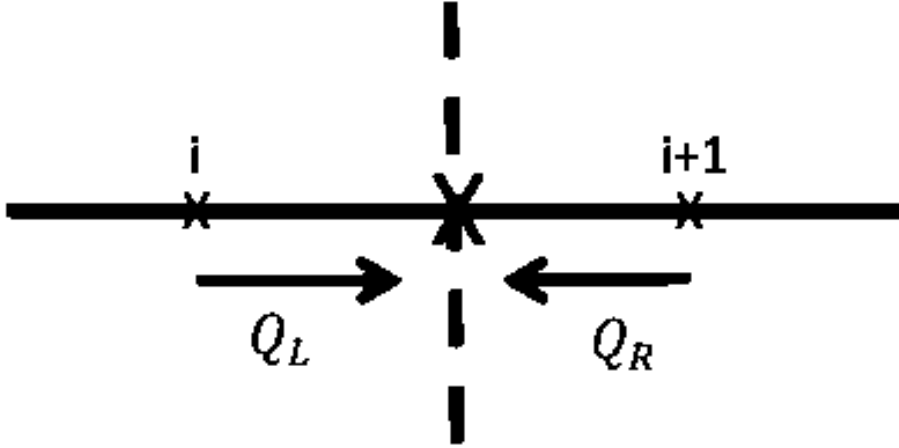


Figure 2.2 : Approaching to point

During the splitting, the point needed is computed by approaching left and right hand side and it shown in Figure 2.2. This approach can be described in (2.14)

$$\frac{\partial Q}{\partial t} + \frac{\partial}{\partial x} (F^+(Q_L)) + \frac{\partial}{\partial x} (F^-(Q_R)) \quad (2.14)$$

This one is the stable and second order. The Van-Leer method is flux terms, which are continuously differentiable through the sonic line and stagnation zones. Left and right term can be shown as,

$$F^\pm = \begin{bmatrix} \pm \frac{1}{4} \rho a (M \pm 1)^2 \\ \pm \frac{1}{4} \rho a (M \pm 1)^2 [(\gamma - 1) Ma \pm 2a] \frac{1}{\gamma} \\ \pm \frac{1}{4} \rho a (M \pm 1)^2 [(\gamma - 1) Ma \pm 2a]^2 \frac{1}{2(\gamma^2 - 1)} \end{bmatrix} \quad (2.15)$$

2.2.2 Roe method

The Roe scheme gives solution on the basis of a localized Riemann problem, which is referred in (Toro, 1999) as district from the Van Leer flux splitting technique. The scheme calculates the flux at a specified face of a solution domain. The basic premise of this problem is that changes in a flow can be transmitted only through entropy waves and acoustic waves, and only at some given speeds, which represent the

eigenvalues of the governing non-linear equation system. In one-dimensional problem, three wave speeds are declared. One of them is the entropy wave at the fluid is traveling, in the upstream and downstream direction, other one is acoustic waves corresponding the speed of sound relative to fluid speed.

As different than Van-Leer method, In Roe Method, additional dissipation part has been added to equation. This operation make equation less diffusive and related error states have been taken out.

$$F = \frac{1}{2} [F^+(Q_L) + F^-(Q_R)] - \hat{T} \hat{\lambda} \hat{T}^{-1} (Q_R - Q_L) \quad (2.16)$$

As seen from (2.16), second part represents dissipation part. Here \hat{T} and $\hat{\lambda}$ are,

$$\hat{\lambda} = \begin{bmatrix} u & 0 & 0 \\ 0 & u + a & 0 \\ 0 & 0 & u - a \end{bmatrix} \quad (2.17)$$

$$\hat{T} = \begin{bmatrix} 1 & 1 & 1 \\ u & 1 & u + a \\ \frac{u^2}{2} & 1 & H + au \end{bmatrix} \quad (2.18)$$

This method is appropriate for catching chock wave. It's not useful for low Mach number.

2.2.3 Solution scheme AUSM+ (Advaction Upstream Splitting Method)

The Advection Upstream Splitting Method (AUSM) is a sound out similarly in bottom to the Van-Leer Method already discussed. Encircling summation, the flux is composed of pair unsociable text consequence divagate each one may be properly upwind stencilled. (Liou, 1996) is the original author of the technique, which has been improved and altered several times since both by them and by others.

In this scheme, fluxes are separated in two parts as,

$$F = \begin{bmatrix} \rho u_1 \\ \rho u_1^2 \\ \rho u_1 u_2 \\ u_1(E + p) \end{bmatrix} + \begin{bmatrix} 0 \\ p \\ 0 \\ 0 \end{bmatrix} \quad (2.19)$$

The first part is convective flux and the second part is pressure flux. Generally is classified like that and also it is a suitable method for low Mach number flow.

Using Finite Volume Method,

$$\frac{\partial Q}{\partial t} + \frac{\partial F_1}{\partial x} + \frac{\partial F_2}{\partial y} = 0 \quad (2.20)$$

Equation can be shown as,

$$\frac{\partial}{\partial t} \begin{bmatrix} \rho \\ \rho u_1 \\ \rho u_2 \\ E \end{bmatrix} + \frac{\partial}{\partial x} \begin{bmatrix} \rho u_1 \\ \rho u_1^2 + p \\ \rho u_1 u_2 \\ u_1(E + p) \end{bmatrix} + \frac{\partial}{\partial y} \begin{bmatrix} \rho u_2 \\ \rho u_1 u_2 \\ \rho u_2^2 + p \\ u_2(E + p) \end{bmatrix} = 0 \quad (2.21)$$

This formulation is converted to integral form,

$$\iint \frac{\partial Q}{\partial t} dxdy + \iint \left(\frac{\partial F_1}{\partial x} + \frac{\partial F_2}{\partial y} \right) dxdy = 0 \quad (2.22)$$

Then it becomes,

$$\iint \frac{\partial Q}{\partial t} dxdy + \oint \vec{n} \cdot \vec{F} ds = 0 \quad (2.23)$$

From discretization it becomes,

$$\frac{Q_i^{n+1} - Q_i^n}{\Delta t} A_e + \sum_{i=1}^4 \vec{n} \cdot \vec{F}(Q_L, Q_R) \Delta S_l = 0 \quad (2.24)$$

Then problem becomes,

$$Q_i^{n+1} = Q_i^n - \frac{\Delta t}{A_e} \sum_{i=1}^4 \vec{n} \cdot \vec{F}(Q_L, Q_R) \Delta S_l \quad (2.25)$$

$\vec{n} \cdot \vec{F}$ term computed from AUSM method it gives result from upwind algorithm. It is explained briefly next sections.

Q_i^n is previous time solution.

A_e , S_l and n terms have been shown on below figure. And also a sample has been demonstrated for a finite volume calculation sequences and node sequences have been selected according to this term.

Here is the,

$$A_e = \frac{\vec{t}_1 \times \vec{t}_2}{2} \quad (2.26)$$

$$\vec{t}_1 = (x(3) - x(1))\vec{i} + (y(3) - y(1))\vec{j} \quad (2.27)$$

$$\vec{t}_2 = (x(4) - x(2))\vec{i} + (y(4) - y(2))\vec{j} \quad (2.28)$$

$$d_{23} = \sqrt{(x_3 - x_2)^2 + (y_3 - y_2)^2} \quad \vec{n}_{23} = \frac{y_3 - y_2}{d}\vec{i} - \frac{x_3 - x_2}{d}\vec{j} \quad (2.29)$$

After that from (Curle, 1955) its solution AUSM+ sequence goes;

$$M_{L/R} = \frac{\vec{n} \cdot \vec{u}_{L/R}}{a_{1/2}} \quad , \quad a_{1/2} = \frac{(a_L + a_R)}{2} \quad , \quad \rho_{1/2} = \frac{(\rho_L + \rho_R)}{2} \quad (2.30)$$

$$\bar{M}^2 = \frac{|\vec{u}_L|^2 + |\vec{u}_R|^2}{2a_{1/2}^2} \quad (2.31)$$

$$M_0^2 = \min(1, \max(\bar{M}^2, M_\infty^2)) \quad (2.32)$$

$$f_a = M_0(2 - M_0) \quad (2.33)$$

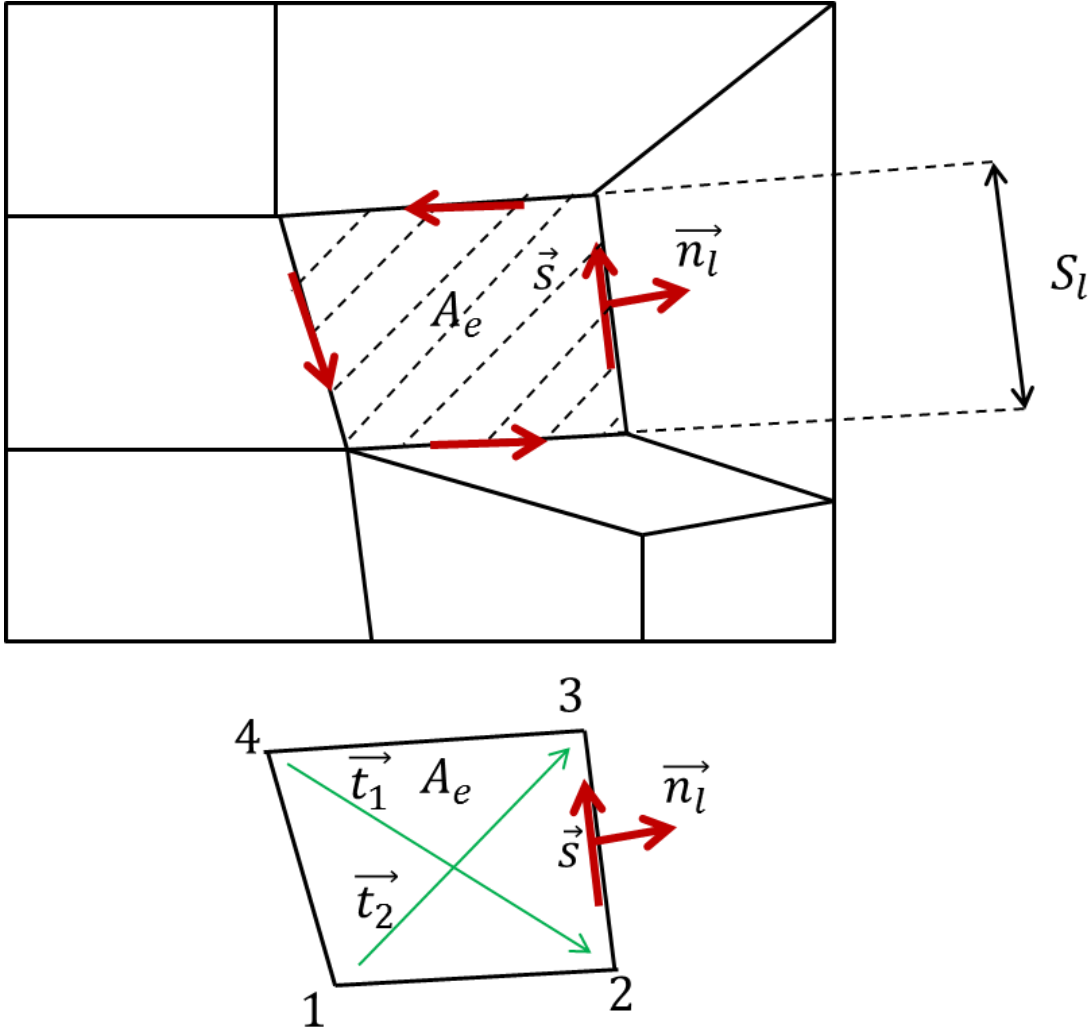


Figure 2.3 :A sample grid structure and notation

$$M_{1/2} = M_{(4)}^+(M_L) + M_{(4)}^-(M_R) - \frac{K_p}{f_a} \max(1 - \sigma \bar{M}^2, 0) \frac{p_R - p_L}{\rho_{1/2} a_{1/2}^2} \quad (2.34)$$

where

$$M_{(4)}^\pm(M) = \begin{cases} \frac{1}{2}(M \pm |M|) & \text{if } |M| \geq 1 \\ \pm \frac{1}{4}(M \pm 1)^2 \left(1 + 16\beta \frac{1}{4}(M \mp 1)^2\right) & \text{otherwise} \end{cases} \quad (2.35)$$

and

$$K_p = 0.25, \sigma = 1, \alpha = \frac{3}{16}(-4 + 5f_a^2), \beta = \frac{1}{8}, K_u = 0.75 \quad (2.36)$$

According to this input, pressure flux,

$$p_{1/2} = P_{(5)}^+(M_L)p_L + P_{(5)}^-(M_R)p_R - K_u P_{(5)}^+(M_L)P_{(5)}^-(M_R)(\rho_L + \rho_R)(f_a a_{1/2}^2)(M_R - M_L) \quad (2.37)$$

and

$$P_{(5)}^\pm(M) = \begin{cases} \frac{1}{2M}(M \pm |M|) & \text{if } |M| \geq 1 \\ \pm \frac{1}{4}(M \pm 1)^2 \left((\pm 2 - M)1 + 16\beta \frac{1}{4}(M \mp 1)^2 \right) & \text{otherw} \end{cases} \quad (2.38)$$

and mass flux,

$$\dot{m}_{1/2} = \begin{cases} a_{1/2} M_{1/2} \rho_L & |M| \geq 1 \\ a_{1/2} M_{1/2} \rho_R & \text{otherwise} \end{cases} \quad (2.39)$$

After that, whole flux can be described as,

$$\vec{n} \cdot \vec{F} = \dot{m}_{1/2} \begin{bmatrix} 1 \\ u_1 \\ u_2 \\ E + p \\ \frac{\rho}{\rho} \end{bmatrix} \begin{matrix} L \\ R \end{matrix} \begin{matrix} \text{if } M_{1/2} > 0 \\ \text{otherwise} \end{matrix} + \begin{bmatrix} 0 \\ p_{1/2} n_x \\ p_{1/2} n_y \\ 0 \end{bmatrix} \quad (2.40)$$

Then, AUSM+ function has set up.

2.2.3.1 Boundary conditions

On solid wall and symmetry condition, due to inviscid flow, pressure values have been set to flux conditions. This value has been taken from closed mesh data as

$$\vec{n} \cdot \vec{F} = \begin{bmatrix} 0 \\ p_L n_x \\ p_L n_y \\ 0 \end{bmatrix} \quad (2.41)$$

Here is the “ L ” represent calculation domain and “ R ” represents neighbour domain.

For inflow boundary condition,

$$\vec{n} \cdot \vec{F} = n_x \begin{bmatrix} \rho_\infty u_\infty \\ \rho_\infty u_\infty^2 + p_\infty \\ \rho_\infty u_\infty v_\infty \\ u_\infty (E_\infty + p_\infty) \end{bmatrix} + n_y \begin{bmatrix} \rho_\infty v_\infty \\ \rho_\infty u_\infty v_\infty \\ \rho_\infty v_\infty^2 + p_\infty \\ v_\infty (E_\infty + p_\infty) \end{bmatrix} \quad (2.42)$$

For outflow condition, it similar to inflow but values is taken from neighbour volume which locating near to outflow.

$$\vec{n} \cdot \vec{F} = n_x \begin{bmatrix} \rho_L u_L \\ \rho_L u_L^2 + p_L \\ \rho_L u_L v_L \\ u_L (E_L + p_L) \end{bmatrix} + n_y \begin{bmatrix} \rho_L v_L \\ \rho_L u_L v_L \\ \rho_L v_L^2 + p_L \\ v_L (E_L + p_L) \end{bmatrix} \quad (2.43)$$

3. AEROACOUSTICS

3.1 Basics of Acoustics

3.1.1 Acoustic perception

Human ears perceive sound by vibrations and motions of molecules in any environment. Most commonly, in air environment, fluid molecules interactions cause to sound conduction and generation. Vibrations occurred in air medium is received by ears and converted to sound information in range of limited frequencies. The range has been determined from 20Hz to 20,000Hz (Errede, 2002).

The intensity of sound is another parameter for describing sound perception. The Intensity range of sound is very large for human. It's represented by sound pressure level (SPL), which increases logarithmically. In literature, to define sound level of sound, a reference sound pressure is predicated. This reference value is taken as,

$$p_{ref} = 20 \mu Pa \quad (3.1)$$

In order to define the loudness of sound, SPL is calculated. Logarithm of root mean square (RMS) of the sound variation per reference pressure value is taken. The calculation is performed logarithmic formulation as shown in below.

$$SPL = 20 \log_{10} \left(\frac{p_{rms}}{p_{ref}} \right) \quad (3.2)$$

The unit of SPL is described in terms of decibels (dB). And, in nature, there are too many various SPL can be observed.

3.1.2 Acoustic sources

In General, acoustic sources can be classified as fluid originated, material friction originated. In this study, aero-acoustic sources are considered. Fluid based sources demonstrate similar characteristic with electromagnetic analogy and fluid mechanics

sources. In aero-acoustics, there are three different sources have been defined which are monopoles, dipoles and quadrupoles.

An acoustic monopole can be described by an example, which would be a small sphere, and radius of sphere expands. A kind of sound wave is radiated by a monopole in all directions equally. Mass inflow fluctuation constitutes monopole noise. In addition, two monopole sources one of them are inhaling motion and another one is exhale motion cause contrast motion which associate turbulent eddies deforming. This formation is called as dipole source, which is occurred near aerodynamic surface. The last one is quadrupole consists of two dipoles. In other words, coaction of turbulent eddies pairs crate quadrupoles (Daniel A. Russell, 1999).

Quadrupoles is only produced by fluctuating stress on the fluid. In literature, for Low Reynolds number, quadrupole component can be neglected.

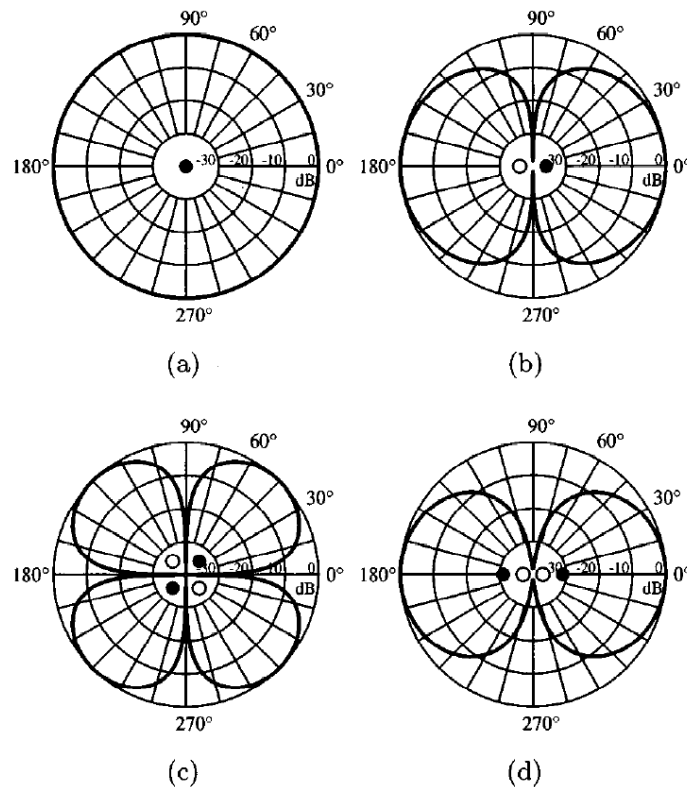


Figure 3.1 :Theoretical directivity patterns for far-field sound pressure levels radiated from (a) monopole, (b) dipole, (c) lateral quadrupole and (d) longitudinal quadrupoles sound sources (Daniel A. Russell, 1999).

3.2 Aeroacoustics Integral Methods

The study of these flow generated acoustic waves probably began with Gutin's theory of propeller noise, which was developed in 1937. Yet, it was not until 1952, when Lighthill introduced his acoustic analogy to deal with the problem of jet noise, which a general theory began to emerge. Subsequently, Curle, Powell and Ffowcs Williams extended Lighthill's ideas, so as to include the effects of solid boundaries. These extensions include Gutin's analysis and, in fact, provide a complete theory of aerodynamically generated sound that can be used to predict blading noise as well as jet noise.

3.2.1 Lighthill's analogy

In this section, Lighthill's aero-acoustics analogy was introduced. Lighthill's approach depends on acoustic radiation of density fluctuation. So as to explain analogy, general government equation is handled for fluid flow such as Continuity equation,

$$\frac{\partial \rho}{\partial t} + \frac{\partial}{\partial x_i}(\rho v_i) = 0 \quad (3.3)$$

momentum equations,

$$\rho \frac{\partial v_i}{\partial t} + \rho(v_i \cdot \nabla)v_i = -\nabla p + \nabla \tau_{ij} \quad (3.4)$$

Here $\nabla \tau_{ij}$ is the viscous part of stress tensor. Multiplying equation (3.3) by v ,

$$v_i \frac{\partial \rho}{\partial t} + v_i \frac{\partial}{\partial x_i}(\rho v_i) = 0 \quad (3.5)$$

and, adding it to momentum equations

$$\frac{\partial}{\partial t}(\rho v) + \nabla(\rho v \times v) = -\nabla p + \nabla \tau_{ij} \quad (3.6)$$

occurs, divergence of equation (3.6) is

$$\nabla \cdot \frac{\partial}{\partial t}(\rho v) + \nabla \cdot \nabla(\rho v \times v) = -\nabla \cdot \nabla p + \nabla \cdot \nabla \tau_{ij} \quad (3.7)$$

Differentiating continuity equation by time,

$$\frac{\partial^2 \rho}{\partial t^2} + \frac{\partial}{\partial t}(\nabla(\rho v)) = 0 \quad (3.8)$$

Subtracting equation (3.8) from (3.7),

$$\frac{\partial^2 \rho}{\partial t^2} - \nabla^2 p + \nabla \cdot \nabla \tau_{ij} = \nabla \cdot \nabla(\rho v \times v) \quad (3.9)$$

To make equation acoustic wave equation, $a_0^2 \nabla^2 \rho$ is subtracted from (3.9),

$$\frac{\partial^2 \rho}{\partial t^2} - a_0^2 \nabla^2 \rho - \nabla^2 p + \nabla \cdot \nabla \tau_{ij} = \nabla \cdot \nabla(\rho v \times v) - a_0^2 \nabla^2 \rho \quad (3.10)$$

Rearrangement of (3.10),

$$\frac{\partial^2 \rho}{\partial t^2} - a_0^2 \nabla^2 \rho = \nabla^2 p - \nabla \cdot \nabla \tau_{ij} + \nabla \cdot \nabla(\rho v \times v) - a_0^2 \nabla^2 \rho \quad (3.11)$$

Then it becomes,

$$\frac{\partial^2 \rho}{\partial t^2} - a_0^2 \nabla^2 \rho = (\nabla \times \nabla)[p_{ij} + \rho v_i v_j - a_0^2 \rho \delta_{ij}] \quad (3.12)$$

As seen from equation (3.11), it is a wave equation. Here δ_{ij} is Kronecker delta function. RHS of equation is source term of wave equation. Equation (3.12) is called Lighthill Equation. It can be written as,

$$\frac{\partial^2 \rho}{\partial t^2} - a_0^2 \nabla^2 \rho = \frac{\partial^2 T_{ij}}{\partial x_i \partial x_j} \quad (3.13)$$

At equation, T_{ij} is called external stress.

$$T_{ij} = p_{ij} + \rho v_i v_j - a_0^2 \rho \delta_{ij} \quad (3.14)$$

and from Lighthill's and Curle's studies, propagation sound can be calculated as,

$$\rho'(x, t) = \rho(x, t) - \rho_0 \quad (3.15)$$

$$\begin{aligned}
&= \frac{1}{4\pi a_0^2} \frac{\partial^2}{\partial x_i \partial x_j} \int \frac{T_{ij} \left(y, t - \frac{R}{a_0} \right)}{R} dV(y) \\
&\quad + \frac{1}{4\pi a_0^2} \frac{\partial^2}{\partial x_i} \int \frac{l_j p_{ij} \left(y, t - \frac{R}{a_0} \right)}{R} dS(y)
\end{aligned} \tag{3.16}$$

Here, $R = |x - y|$, x is observation point, y is the point where acoustic sound is generated, l_j unit direction vector of solid boundary and t is current time. First part of (3.19) is regarding external volume (V) integral that has been created by Lighthill for quadrupole distribution on volume. Second part of equation (3.16) is regarding surface integral (S), which has created by Curle. By this approach total sound generation has been evaluated. In addition to this approach, density propagation should be converted to pressure propagation to solve sound exactly.

Using,

$$dp = a_0^2 d\rho \tag{3.17}$$

$$p'(x, t) = p(x, t) - p_0 \tag{3.18}$$

$$\begin{aligned}
&= \frac{1}{4\pi a_0^2} \int \frac{\partial^2}{\partial t'^2} \frac{(x_i - y_i)(x_j - y_j)}{R^3} T_{ij}(y, t') dV(y) \\
&\quad + \frac{1}{4\pi a_0^2} \int \frac{(x_i - y_i) l_j}{R^2} \frac{\partial p_{ij}(y, t')}{\partial t'^2} dS(y)
\end{aligned} \tag{3.19}$$

From this pressure propagation can be evaluated.

The quantities that can be estimated by the human ear, or measured by other phase-insensitive instruments, are the intensity at any point, and its frequency spectrum. The intensity of sound at a point where the density is ρ is a_0^3/ρ_0 times the mean-square fluctuation of ρ .

$$I(x) = \frac{a_0^3}{\rho_0} \overline{(\rho(x) - \rho_0)^2} \quad (3.20)$$

By using ρ and p relation it can be rewritten as,

$$I(x) = \frac{1}{\rho_0 a_0} \overline{(p(x) - p_0)^2} = \frac{1}{\rho_0 a_0} \langle p'^2 \rangle (x) \quad (3.21)$$

The unit of I are W/m^2 . Intensity of sound ($I(x)$) represents the acoustic energy received at point x in the unit time and per unit area. If $I(x)$ is integrated around a large surface, the acoustic power value radiated from the surface can be calculated totally.

We should define mean-square acoustic pressure from auto-correlation of the acoustic pressure,

$$\langle p'^2 \rangle (x, \tau) = \lim_{T \rightarrow \infty} \int_{-T/2}^{T/2} p'(x, t) p'(x, t + \tau) dt = C(\tau) \quad (3.22)$$

For $\tau = 0$,

$$\langle p'^2 \rangle (x, 0) = \langle p'^2 \rangle (x) \quad (3.23)$$

occurs.

Derived equations and results can be applied to flow without solid boundaries. In solid boundary application reflection cannot be predicted correctly by this methodology. High supersonic jets, low-speed jets can be treated by Lighthill's equations. Lighthill's equation and approach is a kind of integral methods.

3.2.2 Ffowcs Williams-Hawkings equations

For the Lighthill's analogy, sound generated aerodynamically was considered with no solid bodies in the source region. Let us now consider a finite volume of space containing a disturbed flow and rigid bodies in arbitrary motion, the surrounding fluid being at rest. Bodies and flow generate sound. In that case it is certainly possible to replace both flow and surfaces by equivalent acoustic sources, assuming that the whole medium is perfectly at rest (Williams & Hawkings, 1969).

This is the foundation of the aero-acoustic analogy as extended by Ffowcs Williams and Hawking (1969). The key assumption is again that no flow-acoustics coupling occurs or the acoustic field does not affect the flow, from which originates the sound. Consequently, this approach is no more valid when some resonant conditions induce an acoustic feedback on the flow.

When the aero-acoustic analogy can be used, the remaining problem is the determination of the equivalent sources. This can be done as follows.

To represent the real medium with flow and obstacles in a convenient way, Ffowcs Williams and Hawking defined an equivalent medium where the rigid bodies are replaced by mathematical surfaces. The inner volume of the surfaces is assumed to contain the ambient fluid at rest. In order to preserve both the kinematics of the flow and the boundary condition of no cross-flow on the surfaces, a discontinuity must be imposed at the surface location, by introducing some mass and momentum sources in the equations of gas dynamics.

Mass and momentum equations are now written as:

$$\frac{d\rho}{dt} + \frac{\partial}{\partial x_i}(\rho V_i) = \rho_0 V_{Si} \delta(f) \frac{\partial f}{\partial x_i} \quad (3.24)$$

$$\frac{d}{dt}(\rho V_i) + \frac{\partial}{\partial x_j}(\rho V_i V_j - \sigma'_{ij}) = -\sigma'_{ij} \delta(f) \frac{\partial f}{\partial x_j} \quad (3.25)$$

In these equations, ρ, V_i are respectively the density and total velocity components of the flow, ρ_0 is the mean density, V_{Si} is the velocity field of a point on the surfaces, δ means the Dirac delta function, $\sigma'_{ij} = \tau_{ij} - (P - P_0)\delta_{ij}$ is the viscous stress tensor (P being the static pressure with mean value P_0) and $f(\vec{x}, t) = 0$ is an equation defining the kinematics of the surfaces. If the normal unit vector on the surfaces is \vec{n} , the boundary condition of no cross-flow is simply:

$$\vec{V} \cdot \vec{n} = \vec{V}_S \cdot \vec{n} \quad (3.26)$$

A formal procedure can now be used to derive an equation for the density fluctuation $\rho' = \rho - \rho_0$ in the following way from (3.24) and (3.25):

$$\frac{\partial^2 \rho'}{\partial t^2} - c_0^2 \frac{\partial^2 \rho'}{\partial x_i^2} = \frac{\partial^2 T_{ij}}{\partial x_i \partial x_j} + \frac{\partial}{\partial x_i} \left(\sigma'_{ij} \delta(f) \frac{\partial f}{\partial x_j} \right) + \frac{\partial}{\partial t} \left(\rho_0 V_{Si} \delta(f) \frac{\partial f}{\partial x_i} \right) \quad (3.27)$$

(3.27) is an exact equation, because it is a reformulation of the general fluid dynamics equations. ρ' and T_{ij} are to be understood in the sense of generalized functions: they are zero inside the mathematical surfaces and equal, respectively, to the density fluctuations and the Lighthill tensor of the flow outside.

The statement of the generalized acoustic analogy follows:

The density fluctuations in the real fluid, in the presence of flow and rigid bodies, are exactly the same as those that would exist in an equivalent acoustic medium perfectly at rest and forced by three source distributions:

-A volume distribution $\partial^2 T_{ij} / \partial x_i \partial x_j$ in outer region of the surfaces, due to the flow

-A surface distribution $\partial / \partial x_i (\sigma'_{ij} \delta(f) \partial f / \partial x_j)$ due to the interaction of the flow with the moving bodies.

-A surface distribution $\partial / \partial t (\rho_0 V_{Si} \delta(f) \partial f / \partial x_i)$ due to the kinematics of the bodies.

As for Lighthill's equation, the formal result cannot be used directly to calculate the sound produced in a practical situation. In fact above equation is not exactly a wave equation, because the density fluctuation is also present in the supposed source terms. But it must reduce to the wave equation at large distances from the source region, where the right hand side vanishes.

3.2.3 Kirchhoff method

Kirchhoff's formulation is, like methods based on the FW-H equation, an integral method. In transonic or supersonic problems where use of the FW-H equation leads to a quadrupole volume integration, the Kirchhoff's method has the considerable advantage of requiring only a surface integration (Kirchhoff, 1983).

This formulation has been formerly used in light diffraction and electromagnetic problems. The first application to high-speed rotation blades was proposed in 1979 by Hawking. However, as it will be explained later, practical applications to realistic

propeller or helicopter rotor cases have been waiting for many years that progress in CFD methods provide accurate input data for the calculation.

3.3 Acoustic Mathematics

3.3.1 Green's theorem

The acoustic analogy has the formal advantage of formulating the complicated problem of the noise generated by flows and rigid bodies in motion in a more standard one, governed by the inhomogeneous wave equation. Assuming that the sources of this equation are previously determined, the solution is given by the Green's function technique. The following section is devoted to this technique. However, since the wave equation is known to describe all problems in physics in which the effect of a potential propagates with a finite speed, the results are presented for any scalar field $\varphi(\vec{x}, t)$, acoustic or not, solution of a wave equation. This will later permit us to distinguish the behaviours respectively due to the equation and to the specific nature of sources in acoustics.

For the sake of generality, assume a given source distribution $S(\vec{x}, t)$ radiating in a volume of space ϑ_t limited by moving rigid surfaces $\Sigma_{(t)}$. The local normal on the surfaces \vec{n} is pointing outwards the volume. The wave equation is:

$$\Delta\varphi - \frac{1}{c_0^2} \frac{\partial^2 \varphi}{\partial t^2} = S(\vec{x}, t) \quad (3.28)$$

Assume further that the solution G is known in the case of an impulse point source in the following sense:

$$\Delta G - \frac{1}{c_0^2} \frac{\partial^2 G}{\partial t^2} = -\delta(\vec{x} - \vec{y})\delta(t - t') \quad (3.29)$$

G is a Green's function of the problem. It depends on four variables and represents the field produced at point \vec{x} and time t by an elementary source at point \vec{y} and time t' .

The standard method to solve the wave equation is fully described, for example, by (Goldstein, 2001). Multiply the first equation by G , the second one by φ , form the difference and integrate with respect to space variables and time. Then introducing

the Green's theorem, the Leibnitz's rule and the causality condition leads to the formal solution:

$$\begin{aligned}
\varphi(\vec{x}, t) = & - \int_{-\infty}^{\infty} \int_{\vartheta_t} G\left(\vec{x}, \frac{t}{\vec{y}}, t'\right) S(\vec{y}, t') d\vec{y} dt' \\
& - \int_{-\infty}^{\infty} \int_{\Sigma(t)} \left\{ G\left(\frac{\partial}{\partial n} + \frac{V_n}{c_0^2} \frac{\partial}{\partial t'}\right) \varphi \right. \\
& \left. - \varphi\left(\frac{\partial}{\partial n} + \frac{V_n}{c_0^2} \frac{\partial}{\partial t'}\right) G \right\} d\Sigma_{\vec{y}} dt'
\end{aligned} \tag{3.30}$$

3.3.2 Fourier transform

The Fourier transform is the most important computational milestone in signal analysis. In thesis scope, continuous time case has been discussed. Filtering, modulation and sampling properties and their meanings have been explained in this section. The first property is symmetrical feature of Fourier transform in imaginary axis. Because of that, displaying of only real values of w is necessary. Second property regards time and frequency scaling. In other words, linear expansion of the time space has the influence in the frequency space of a linear expansion. Another parameter is duality of time and frequency domains. That means, the Fourier transform of the Fourier transform equals to signal reversed of original signal in time. Also, there is another property that's Parseval's relation. It's called time-shifting property also. This property shows that the differentiation in time equals to linear phase factor in the frequency domain (Randall, 1987).

The general case by letting $T \rightarrow \infty$, in which case the spacing $1/T$ between the harmonics tends to zero and $G(f)$ becomes a continuous function of f . It can be shown that,

$$G(f) = \int_{-\infty}^{\infty} g(t) e^{-j2\pi f t} dt \tag{3.31}$$

and time base equation becomes,

$$g(t) = \int_{-\infty}^{\infty} G(f) e^{j2\pi f t} df \tag{3.32}$$

Equation (3.31) is known as the “forward” transform and equation (3.32) as the “inverse” transform while together they form the “Fourier Transform Pair”. It can be seen that they are almost symmetrical. The only difference is the sign of the exponent of e . The most important thing about the symmetry is that results, which apply to transformation in one direction generally, also apply to transformation in the other direction (Randall, 1987).

The final possibility occurs when the functions are sampled in both time and frequency domains. Because of the sampling, it is evident that both time signal and frequency spectrum are implicitly periodic in this case, and this periodicity leads to some interesting effects.

The forward transform now takes the form,

$$G(k) = \frac{1}{N} \int_{n=0}^{N-1} g(n) e^{-j \frac{2\pi f t}{N}} \quad (3.33)$$

and the inverse transform takes the form,

$$g(n) = \int_{k=0}^{N-1} G(k) e^{j \frac{2\pi f t}{N}} \quad (3.34)$$

Because the infinite continuous integrals of equations (3.31) and (3.32) have been replaced by finite sums, the above transform pair, known as the “Discrete Fourier Transform” or DFT, is much better adapted to digital computations. Even so, it can be seen that in order to obtain N frequency components from N procedure, known as the “Fast Fourier Transform” or FFT algorithm, which obtains the same result with a number of complex multiplications of the order of $N \log_2 N$. The reduction factor in computation time is thus of the order of $N / \log_2 N$, which for the typical case of $N = 1024(2^{10})$ is more than 100.

Re-writing equation (3.33) as,

$$G(k) = \int_{n=0}^{N-1} g(n) W_N^{nk} \quad (3.35)$$

It is easy to realise that the same values of W_N^{nk} are calculated many times as the computation proceeds. Firstly, the integer product nk repeats for different combinations of k and n ; secondly, W_N^{nk} is a periodic function with only N distinct values (Randall, 1987).

3.3.3 Nyquist criteria

In project scope, acoustic perturbation data has been converted to noise magnitude (dB) vs. frequency to understand noise characteristic. In this perspective, to obtain sufficient data quality, Nyquist criteria has been utilized.

The Nyquist sampling theorem provides a prescription for the nominal sampling interval or in required avoiding aliasing. It may be stated simply as follows:

The sampling frequency should be two time of highest frequency of total signal. It can be described as,

$$f_s \geq 2f_c \quad (3.36)$$

Where f_s represents the sampling frequency and f_c represents the highest frequency in problem. (Nyquist, 2002)

3.3.4 Strouhal number

To show noise characteristic as a dimensionless value, Strouhal number is used in literature. Independent from flow condition, acoustic characteristic can be estimated from that value.

Strouhal number can demonstrate different characteristic according to flow regime. For instance, in viscosity dominant flow, flow oscillation occurs in collective flow collision by large Strouhal number and in high-speed flow, flow oscillation is provided by quasi-steady state component of flow by small Strouhal number. The Strouhal number given in Fig. 15 is defined as:

$$St = \frac{f_v D}{V} \quad (3.37)$$

where f_v is the vortex shedding frequency, D is the tube diameter and V is the flow velocity (Oengoeren, 1998).

4. STUDY DESCRIPTION

4.1 Base Study

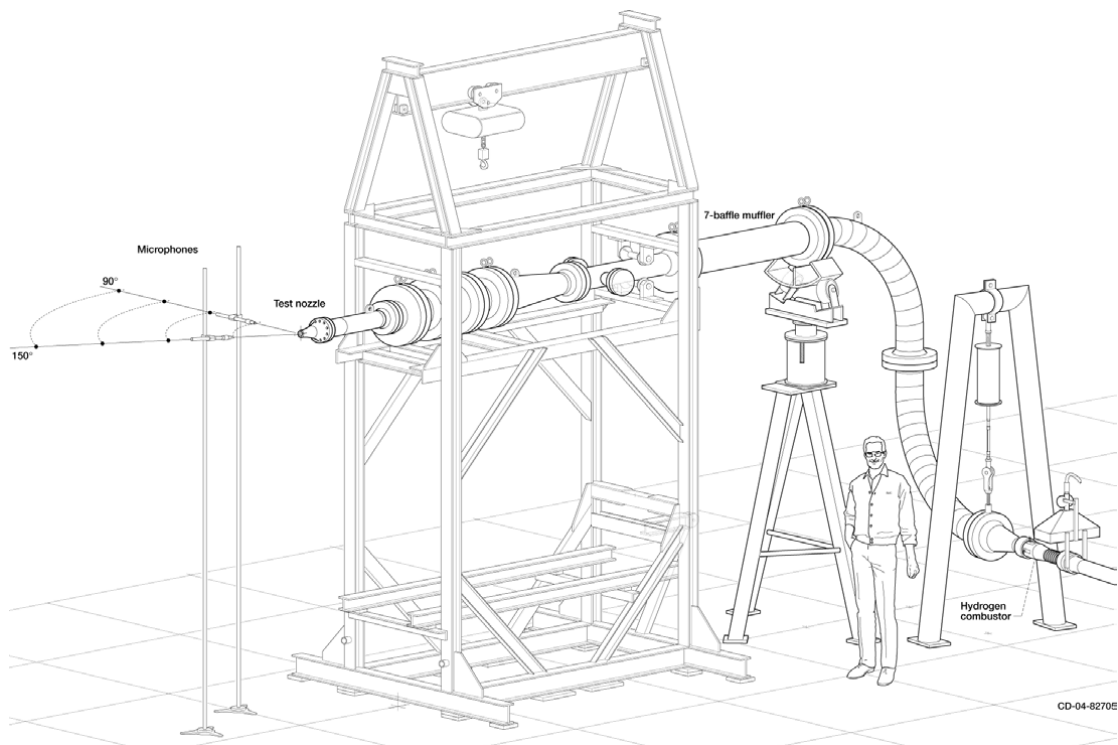


Figure 4.1 : Small hot jet acoustic rig (SHJAR) (Bridges, Acoustic Measurements of Rectangular Nozzles with Bevel, 2012)

As declared in (Bridges, Acoustic Measurements of Rectangular Nozzles with Bevel, 2012), reference test result has been obtained from Small Hot Jet Acoustic Rig (SHJAR) located in the Aero-Acoustic Propulsion Laboratory (AAPL) in NASA cooperation. The SHJAR was set up for supporting jet noise studies. In this place, from the centreline of jet exit, at 3.81 arc radius, acoustic measurements are performed. Totally 24 microphones are sequenced with 5 degree equal interval from 50 degrees to 165 degrees. During the test process, the ambient temperature, pressure and relative humidity and acoustic sources are recorded. By 0.5-percentage error factor, Mach number and static temperature ratio are calculated. In addition, ± 0.2 dB repeatability exists in 1/3 octave band.

The rig has 2.7 kg/s mass flow rate capacity and maximum temperature limit is 980K. The rig was designed according to a several criteria that are without swirl effect and no separation region at inner surfaces.

In this study, a real nozzle has been investigated. For the beginning NA2Z convergent small jet has been handled. As seen from 3D figure of NA2Z nozzle, nozzle has a 2:1 aspect ratio.

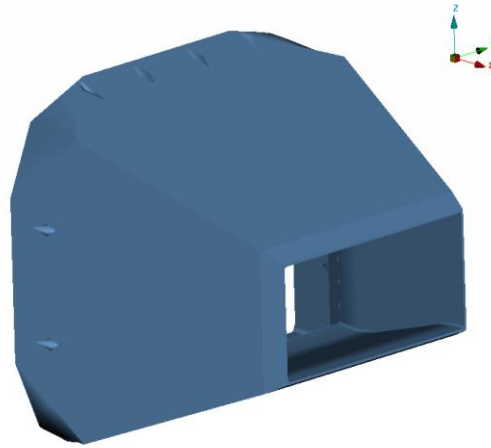


Figure 4.2 : NA2Z convergent nozzle

From $y=0$ section, 1:1 scale dimensions of nozzle have been shown in Figure 4.3. In thesis scope, non-dimensional numbers have been used. From this perspective, it has $1 \times D_{NE}$ exit and $2.47 \times D_{NE}$ inlet. Total length is $2.58 \times D_{NE}$ as seen on figure. D_{NE} represents exit diameter of nozzle.

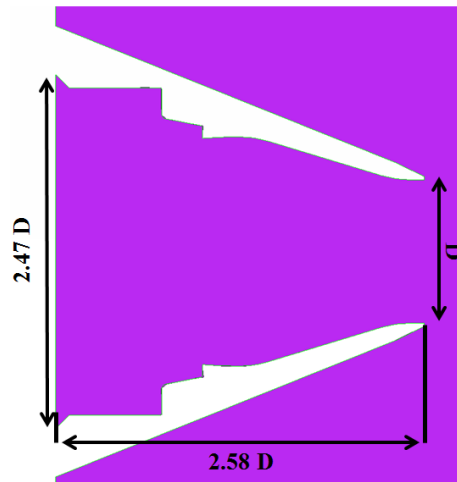


Figure 4.3 : Dimensions of nozzle

Numerical results that are obtained from nozzle exit are shown as frequency vs. dB scale. According to microphone location, the result can show different characteristics. The main effective factor is an azimuth angle for that approach. As seen from below figure, azimuthal angle is measured by the difference from the perpendicular line of the centreline of jet. Microphone locations have been set according to this information. Generally, numerous microphones are put in generic points described by distance from centreline and azimuthal angle.

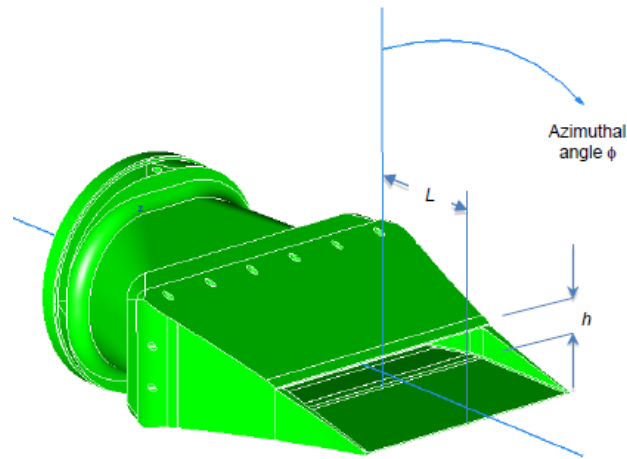


Figure 4.4 :Notation of microphones location angles

According to test results of NA2Z at test rig, a graphical result has been obtained as below. Test condition was defined as an unheated state (Bridges, Acoustic Measurements of Rectangular Nozzles with Bevel, 2012). Data contains a test data comparison of NA2Z, GTRI and SMC000, which are similar to experimental nozzle shape.

As seen on Figure 4.5 acoustic noise levels have been shown in terms of SPL corresponding Strouhal dimensionless number mentioned in section 3 (Seiner, 1984). In project scope, turbulence calculation does not exist. And screech tone represents vibration sourcing from the nozzle edge and trailing edge structure. As an assumption, this kind of source has been neglected. Therefore, only broadband shock noise data will be handled with simulation result obtained from in-house code.

In addition, a reference study provided by Nichols has been demonstrated in Figure 4.6. According to study, the effect of the mesh resolution to solution has been figured out. Mesh resolution is an effective component for modelling at shock noise region. The same screech tone has been obtained for each condition.

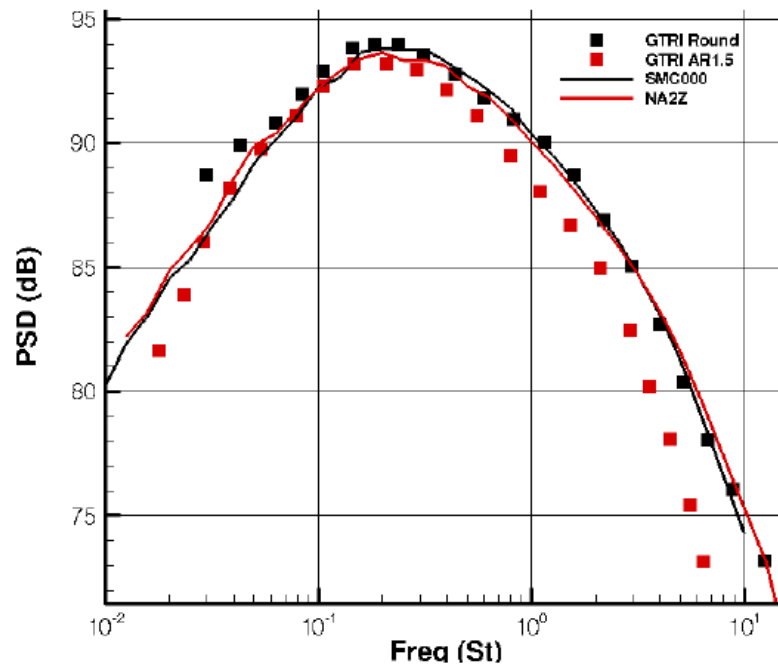


Figure 4.5: Result of NASA test in terms of frequency vs dB

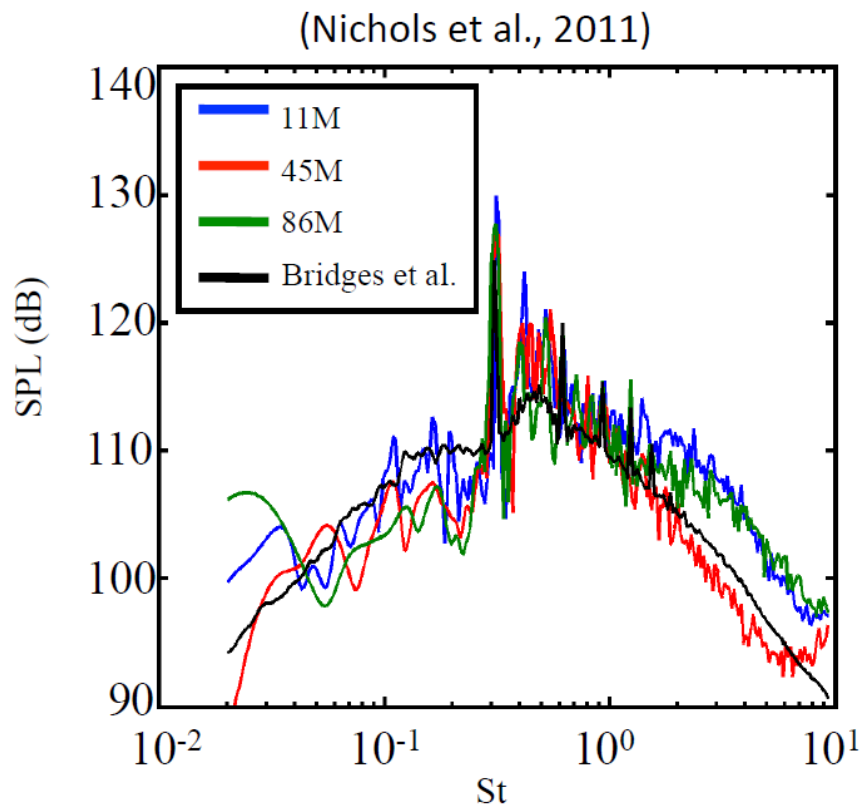


Figure 4.6: Reference simulation result for mesh resolution effect

4.2 Model Setup and Solution Scheme

LEE Model used in the project has been modelled in 2-dimensional. Assessment of flow has been performed according to 2-dimensional data. The first assumption is derived from this approach. The assumption is the third dimension neglecting. From this point, a section of the nozzle has been taken. Y-zero section of the nozzle has been found as appropriate to represent nozzle correctly. The section from the middle of the nozzle interior and the outer medium has been evaluated. Sequence of section generation has been shown on below figure.

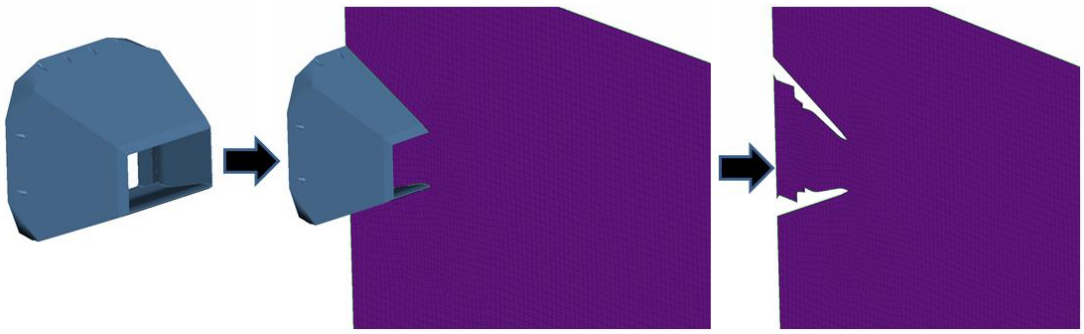


Figure 4.7 : Generation of 2D section

For first assessment, upward, downward, inlet and outlet boundary have been set. Upward and downward wall have been defined as symmetry boundary condition. The far field wall has been defined as outflow. The wall given as flow entrance has been defined as velocity inlet. Whole these definitions have been shown on below figure. To show some feature characteristic according to a unique reference length, nozzle exit diameter has been referred and it's called as D_{NE} in this thesis. Thus, Outflow boundary has been positioned $20 \times D_{NE}$ far from velocity inlet and symmetry boundaries are located at $3.5 \times D_{NE}$. Accordingly, total domain borders have been shaped as below.

Grid model has been performed ANSA meshing program which is used commercially lots of industrial company. Grids used in model have been generated as a fully quad element due to the generated methods nature working with structured mesh. In mesh model, some restriction is concerned. One of them is called as “min/max angle quad criteria” which represents the controlling angle at each vertex (Fluent Inc., 2002). The restriction has been shown at below equation and figure.

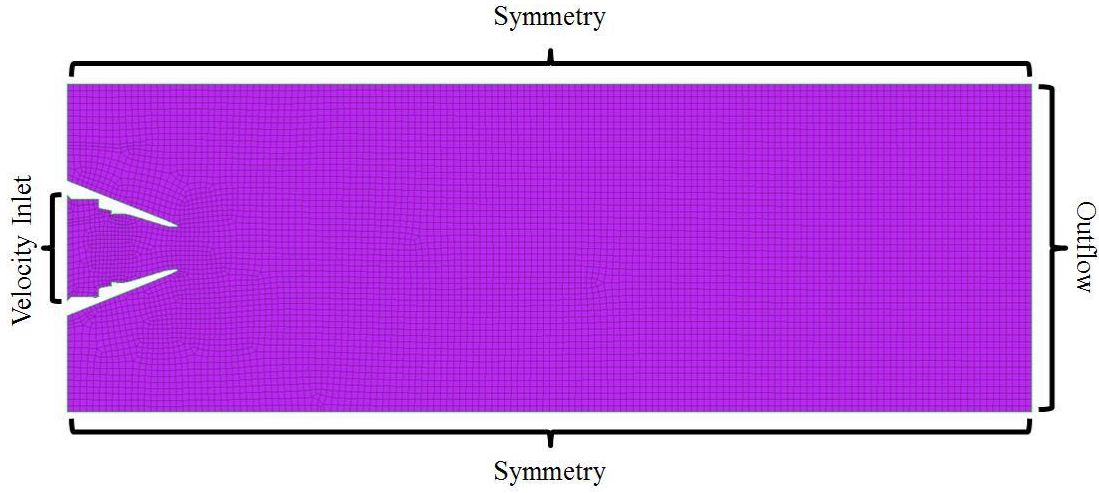


Figure 4.8 : Boundary conditions of domain

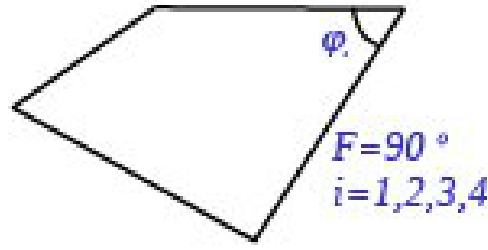


Figure 4.9 : Angles of quad element

$$Angle = \max\left(\frac{\max(\varphi_i) - F}{180 - F}, \frac{F - \min(\varphi_i)}{F}\right) \quad (4.1)$$

For first assessment, domain has been modelled with equal mesh size and totally 8272 grids have been used. The output file is exported as “.inp” type file a kind of ABAQUS extension includes node coordinates and grid-node matches. However, there is not any neighbour data in the file content. After mesh generation, to execute main solver code, neighbours of each grid should be found. To explain this sentence, below figure can support for grid detail. Each grid has four neighbour elements and edge. In grid structure, vertices in grid sequence in clockwise direction. According to this information, a neighbouring code has been generated. On code structure, searching is performed for common vertices and neighbour elements have been found. Related pseudo code can be found from Figure 4.11.

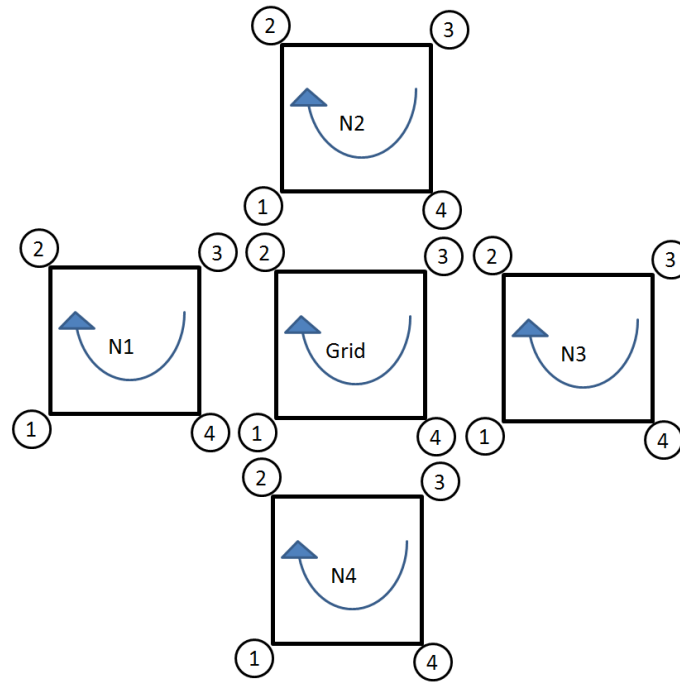


Figure 4.10 : Grid structure

```

• Pseudo code:
CN=cell number
NE=Neighbor element
Gn1=1. node of grid
Gn2=2. node of grid
Gn3=3. node of grid
Gn4=4. node of grid
Nn1=1. node of element
Nn2=2. node of element
Nn3=3. node of element
Nn4=4. node of element
for CN=1:N
    for NE=1:N
        for i=1:4
            for j=1:4
                if Nn(i)==Gn(j)
                    #first node is common search
                    #2nd node
                    if Nn(i+1)==Gn(j-1)
                        #2nd node is found and
                        #this is neighbour element
                    end
                end
            end
        end
    end
end
end

```

Figure 4.11 : Neighbouring pseudo code

```

Read Mesh Vetices
for  $i \leftarrow 1$  to  $np$  do
| read  $x[i], y[i], z[i]$ 
end

Read Element Connectivity
for  $i \leftarrow 1$  to  $ne$  do
| read  $nec[i,1], nec[i,2], nec[i,3], nec[i,4]$ 
end

Read Neighbouring Element Numbers
for  $i \leftarrow 1$  to  $ne$  do
| read  $fec[i,1], fec[i,2], fec[i,3], fec[i,4]$ 
end

Initial Q Value
 $Q^1 := Q_\infty$ 

Time integration
for  $Time \leftarrow 0$  to 4 do
|
|   Compute  $Q^{n+1}$ 
|   for  $i \leftarrow 1$  to  $ne$  do
|   |  $RHS := 0$ 
|   | for  $n \leftarrow 1$  to 4 do
|   | | ....
|   | | ....
|   | | ....
|   | | if Solid Wall Boundary Condition then
|   | | | ....
|   | | |  $RHS := RHS + \dots$ 
|   | | else if Inflow Boundary Condition then
|   | | | ....
|   | | |  $RHS := RHS + \dots$ 
|   | | else if Outflow Boundary Condition then
|   | | | ....
|   | | |  $RHS := RHS + \dots$ 
|   | | else
|   | | |  $Q_L = \dots$ 
|   | | |  $Q_R = \dots$ 
|   | | |  $n_x = \dots$ 
|   | | |  $n_y = \dots$ 
|   | | | call AUSM_Flux( $Q_L, Q_R, n_x, n_y, \mathbf{n} \cdot \mathbf{F}$ )
|   | | |  $RHS := RHS + \mathbf{n} \cdot \mathbf{F} \dots$ 
|   | | end
|   | |  $\Delta Q :=$ 
|   | end
|   |  $Q^{n+1} := Q^n + \Delta Q$ 
| end
end
end

```

Figure 4.12 : Main program pseudo code

By the output of neighbouring code, main code can be executed. From the section 2.2.3 , code structure has been set up as shown in Figure 4.12. For initial condition of domain has been taken as below equation.

$$u(1:N) = 3M, v(1:N) = 0, p(1:N) = 101325, \rho(1:N) = 1.225 \quad (4.2)$$

$$CFL = u \frac{dt}{dx} + v \frac{dt}{dy} < C_{max} \text{ and } C_{max} = 1 \quad (4.3)$$

Thus, stabilization problem and divergence problem during analysis is solved. At this problem, using this approach, time step has been taken as 0.00001s.

In Figure 5.6, main program code fundamentals have been shown. Answer of “How does the program work?” and “main solver scheme” can be found from below figure.

5. RESULTS

5.1 Aerodynamic Assessments

From benchmark result obtained from FLUENT by using same mesh structure demonstrates similar results. This similarity shows that output derived from In-house developed code has consistency and alignment with FLUENT. In cases, density distribution and pressure distribution show dramatic changes on flow variable. However, to represent acoustic pressure detail, output data is not appropriate for assessment. Due to this reason, additional mesh and model refinement have been regenerated.

As seen in Figure 5.1 and Figure 5.2, domain sizes have been changed to prevent reverse flow at boundaries and catch acoustic part as proper. Total length of domain has been increased from $20 \times D_{NE}$ to $40 \times D_{NE}$. And, total width has been changed from $3.5 \times D_{NE}$ to $8 \times D_{NE}$. By increasing domain size, grid number also has increased. By new mesh structure, totally 11656 grids have been used.

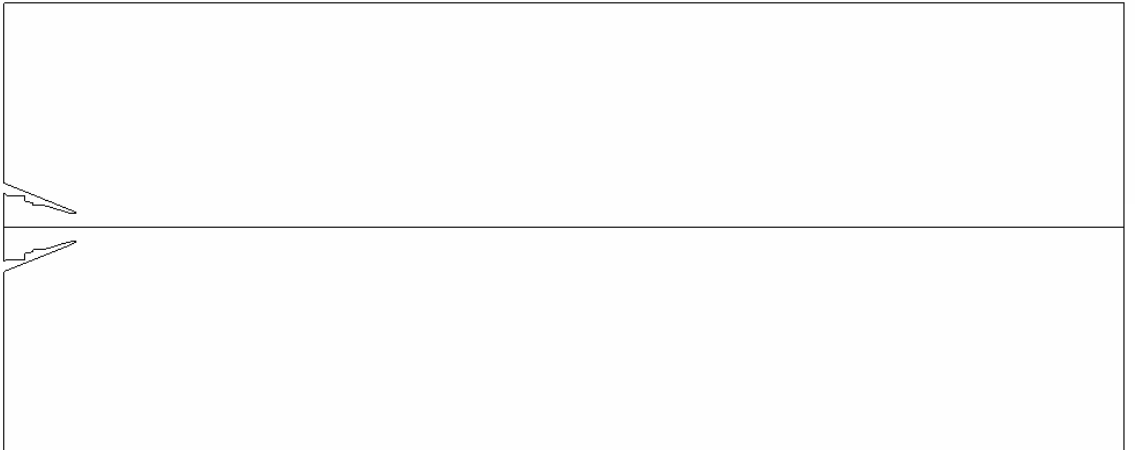


Figure 5.1 : Refined solution domain (2nd assessment)

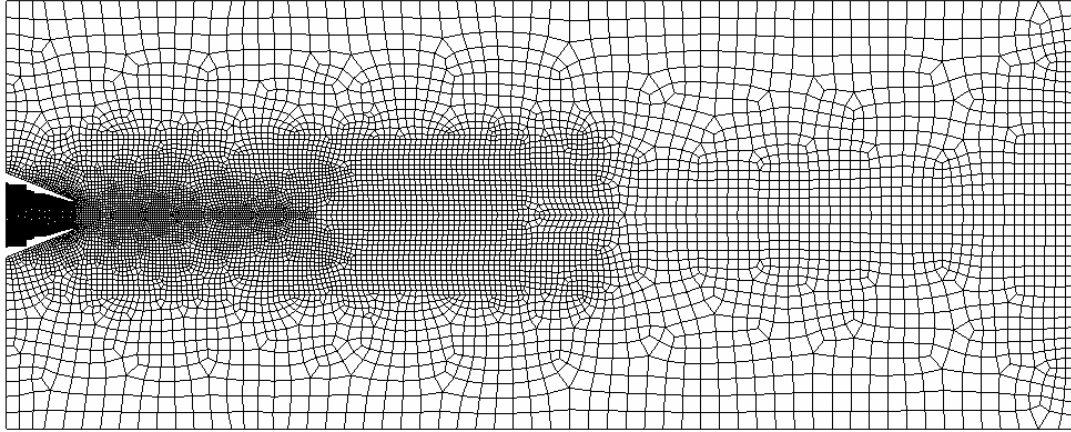


Figure 5.2 : Refined mesh resolution (2nd assessment)

After re-meshing domain and redefining boundaries, the solution has been executed again. As mentioned before, by taking time interval as 0.00001s, analysis has been compiled. To observe maturity of flow event, pressure and velocity data have been collected from the centreline points on domain. Result of plotting pressure vs. time and velocity vs. time; observation has been performed from Figure 5.3 and Figure 5.4. From this analysis, at $t=0.460s$, flow has become fully developed situation.

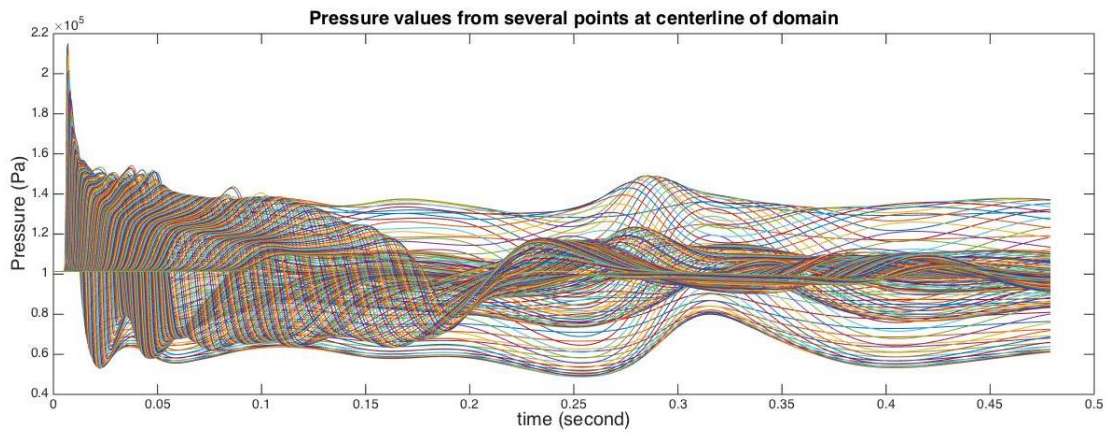


Figure 5.3 : Pressure values vs time from centreline points

Code generation and post process have been performed in MATLAB. However, Due to need of more technical and detailed post-process, TECPLOT has been used for post-processor. From the output of main code has been imported from TECPLOT and flow visualize has been performed as seen in figures below.

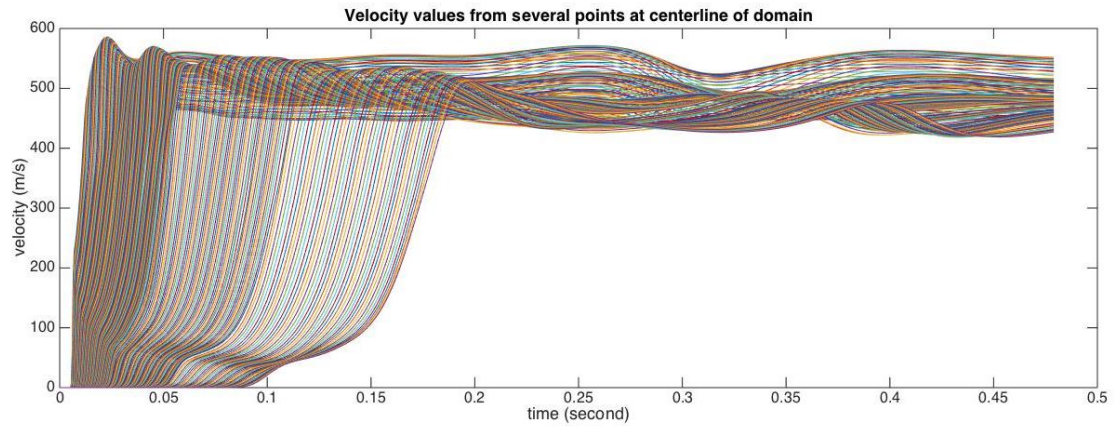


Figure 5.4 : Velocity values vs time from centreline points

As of the second of 0.48300, results have been observed. New results include much more detail according to first assessment. In Figure 5.5, pressure distribution of flow has been shown. Right-hand side and left-hand side of shock wave and its dramatic changes have been simulated. Shock wave locations and types can be predicted correctly by this method. Shock structure is located centreline and far away from exterior borders. From that perspective, domain size seems sufficient to simulate this kind of problem.

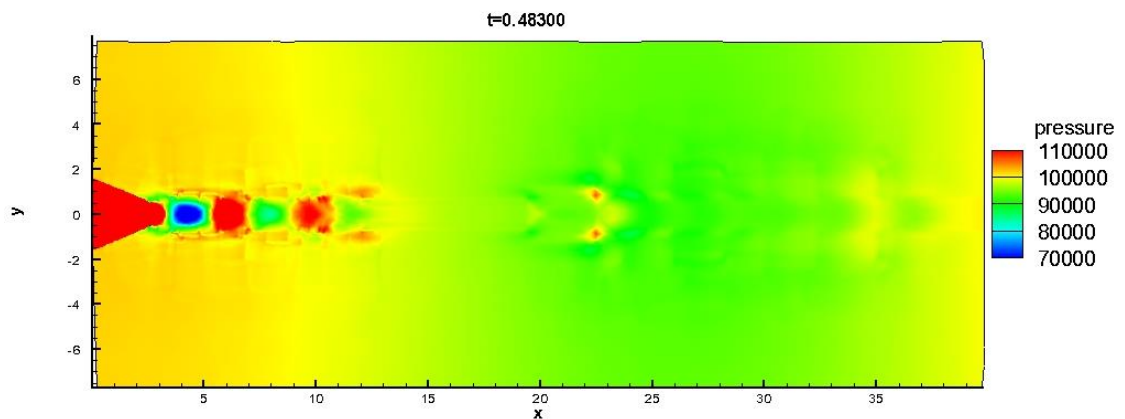


Figure 5.5 : Pressure distribution of domain at time equals to 0.48300

As seen from Figure 5.5, strong pressure gradient has occurred, especially near to nozzle exit. To review flow region deeply, another figure has been shown in Figure 5.6. The main goal is explaining shock structure, so, colour spectrum has been arranged according outer shock structure not interior shock happening in the nozzle.

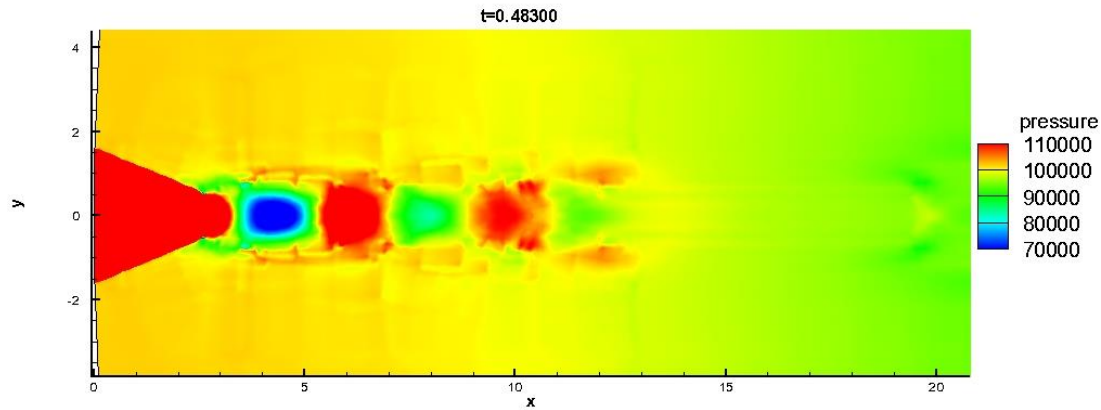


Figure 5.6 :Pressure distribution of domain at time equals to 0.4830 near to nozzle exit

In Figure 5.6, pressure data has been shown. Here, pressure gradient, normal shock, oblique shock wave can be observed. Oblique shock waves, Mach disks have been located on one domain after another. The flow event is a kind of over the expanded jet in other hand, pressure value of the interior of the nozzle is lower than ambient pressure. After 5th pack flow regime has been converted to w/o shock regime. Pressure values have been distributed smoother in that area. From literature, the normal over expanded jet characteristics have been found. The output figure obtained from code and literature seems aligned. The code output verifies about correction of solution scheme.

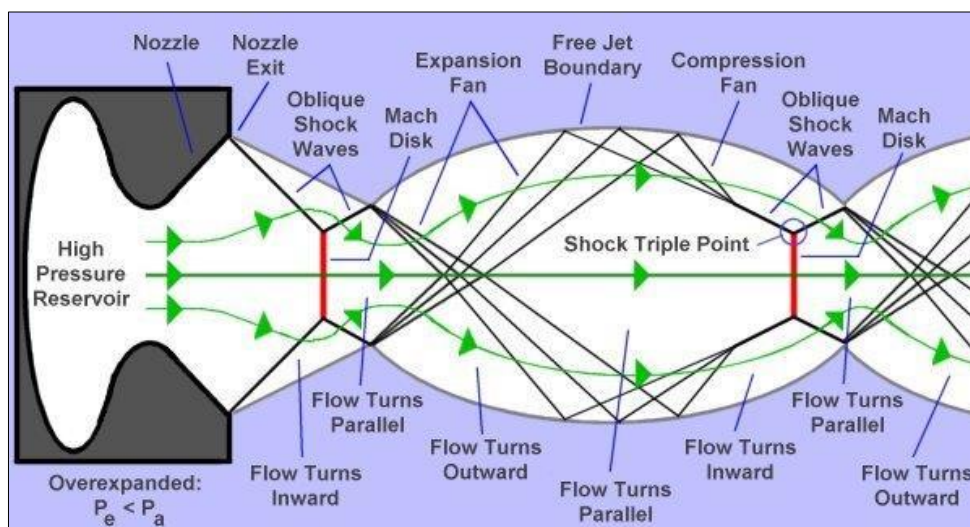


Figure 5.7 : Overexpanded jet characteristics

In addition, density distribution also has been shown in Figure 5.8. Density gradient also shows the shock wave location. Similarly, dramatical effects caused by shock have been shown in that figure. Due to overexpanded jet case, nozzle interior density is higher than the exterior domain density.

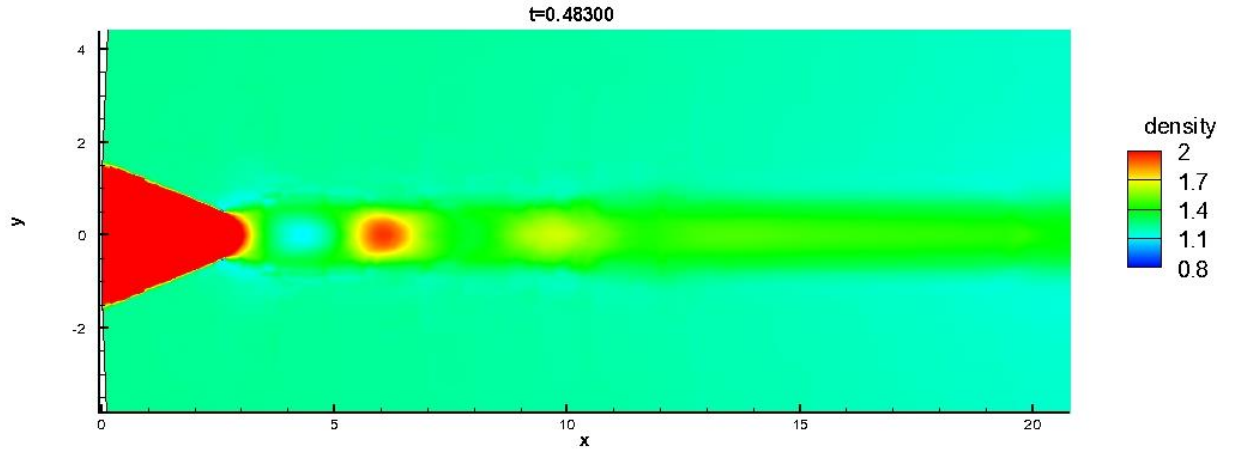


Figure 5.8 : Density distribution of domain at time equals to 0.4830 near to nozzle exit

In Figure 5.9, velocity regime has been demonstrated. The free jet boundary has been figured out clearly. Although, inlet velocity is given as 1020 m/s, nozzle interior velocity is not higher than 340m/s that equals to Mach Number. That case is a rule of supersonic nozzle condition. After the exit, flow reaches to the supersonic level. From exit to outflow boundary, supersonic velocity condition is conserved. From velocity profile, domain size seems sufficient again.

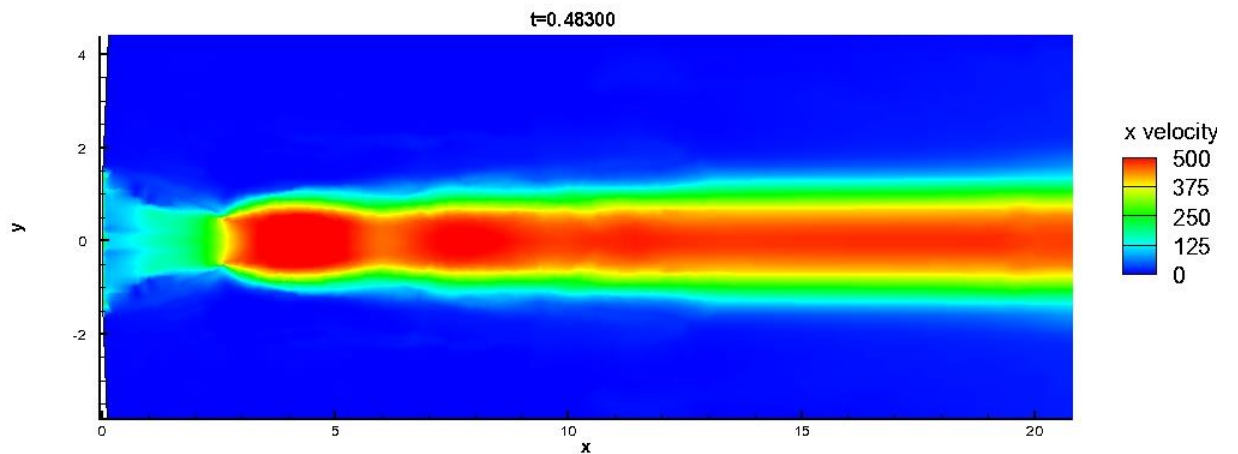


Figure 5.9 : Velocity distribution of domain at time equals to 0.4830 near to nozzle exit

Aerodynamic assessment also has been compared with FLUENT output handled from 0.4 second. According to benchmark data, variable distribution on domain shows similar characteristics. However, the region exit of nozzle shows different characteristics. Deeply, current mesh resolution is not proper for FLUENT case even though it works for in-house code.

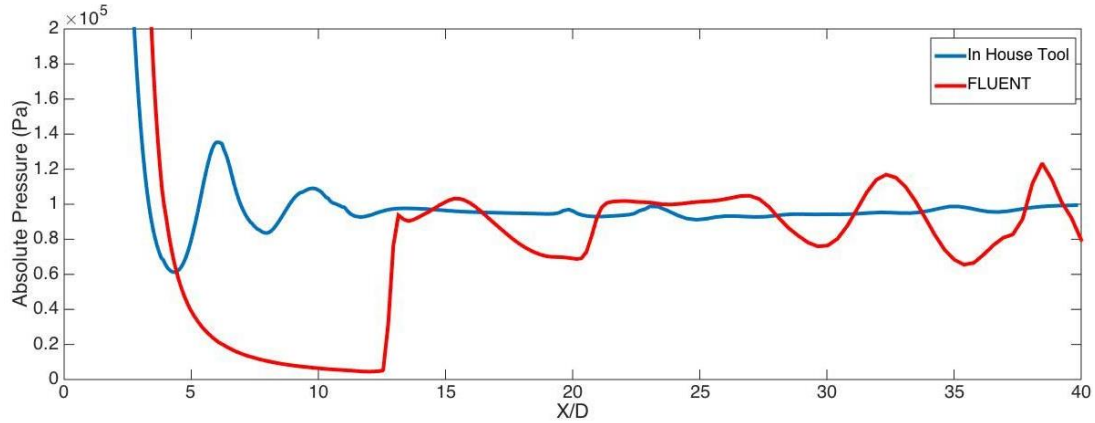


Figure 5.10 : Benchmark study for pressure values at centerline t=0.4

5.2 Acoustic Assessments

Acoustic determinations have been executed using frequency approaches of Nyquist principles and reference case resolution. In this perspective, time step size has been taken as 0.00001 second. Moreover, acoustic record has been performed for 0.65 second totally. By this approach, 50 kHz resolution data gathering has been provided. By taking 0.2s data for initialization, the calculation has been performed. Between 0.85 seconds, data acquisition has been performed.

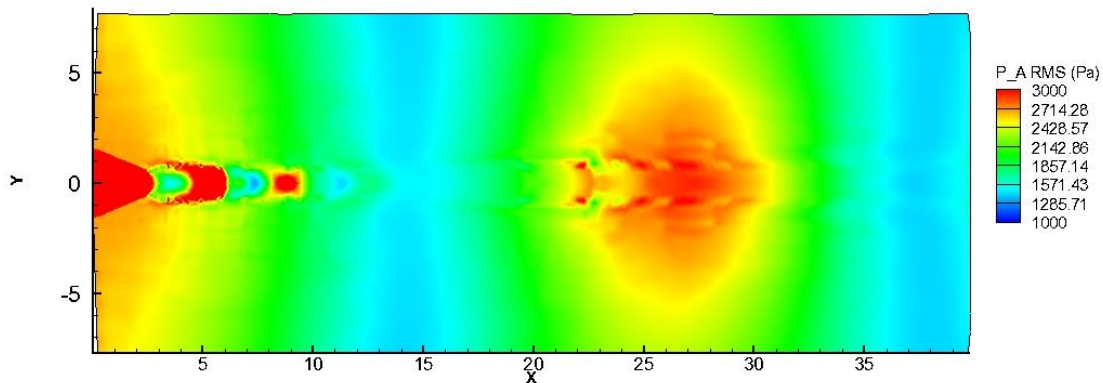


Figure 5.11 : Acoustic pressure fluctuation field (Pressure RMS) (0.4s-0.8s)

To understand the effectiveness of locations in terms of acoustic perturbation, pressure fluctuation has been calculated in time, space, which is between 0.4s and 0.8s. Time pressure fluctuation graphs have been obtained and figured out in Figure 5.11. The figure demonstrates dominant region from the fluctuation point of view. Fluctuation gives hints for acoustic wave propagation. From the figure, interior of the nozzle, 2nd and 4th shock centre and the far field region near to $25 \times D_{NE}$ section.

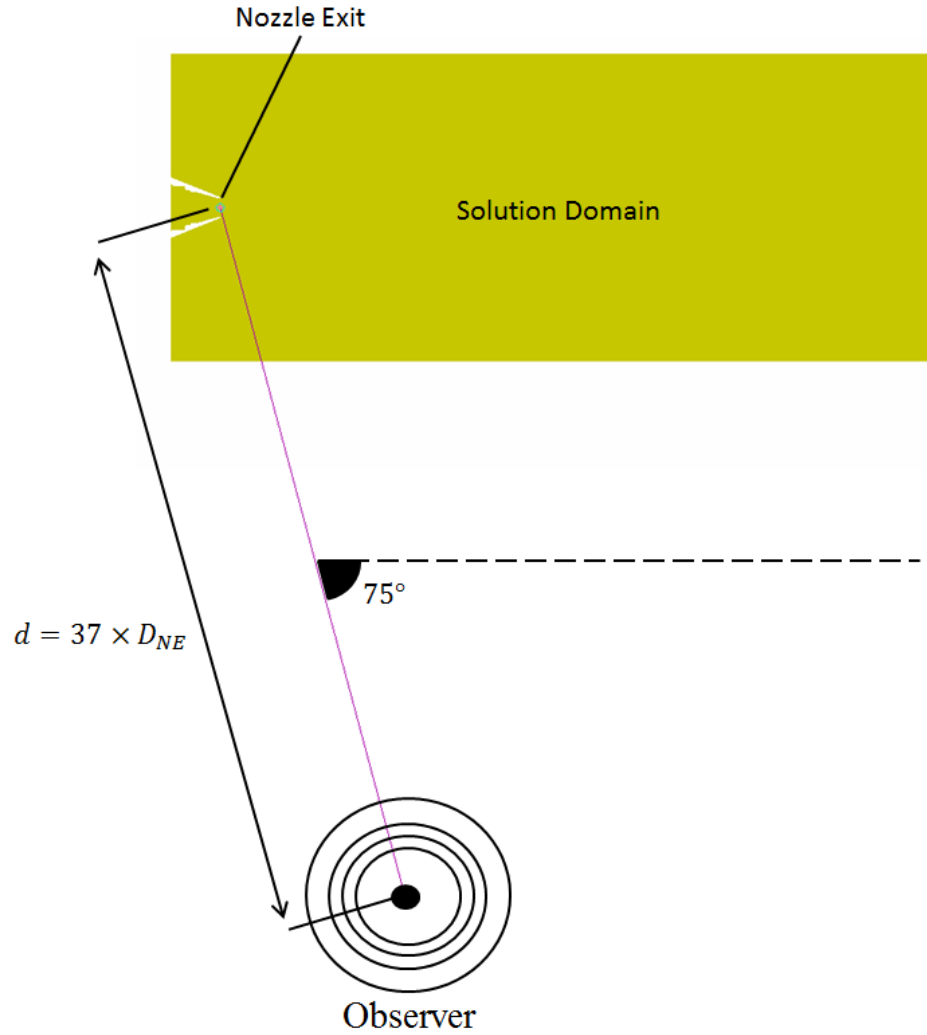


Figure 5.12 : Microphone locations based on reference

As seen in Figure 5.12, microphone location has been shown as a node position near to nozzle exit. Summation of pressure fluctuation of whole grid structure respect to microphone position is calculated using appropriate algorithm that is Lighthill's analogy. As mentioned before, considered problem does not include any turbulent

term, any additional reflective surface and viscous terms. So, Lighthill's analogy has been found the most proper methodology for the project.

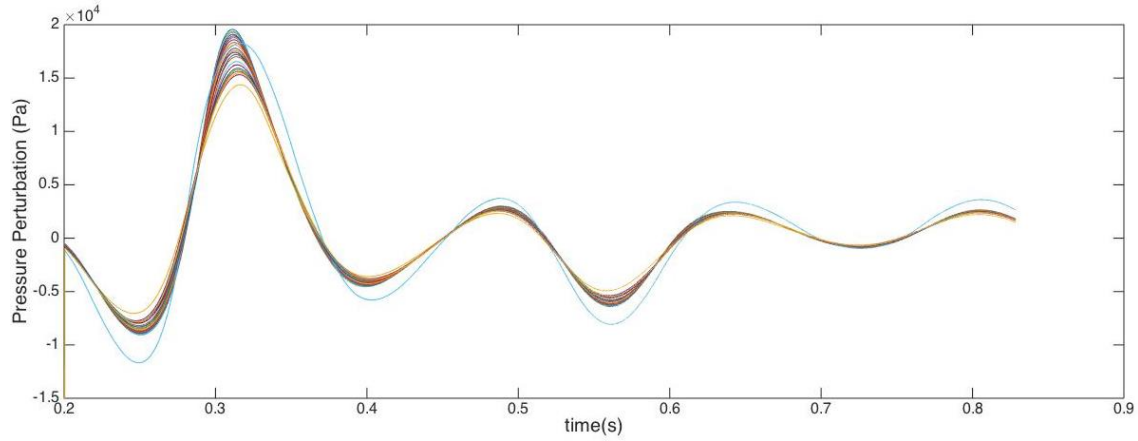


Figure 5.13 : Pressure perturbation of microphone points

And, at whole microphone point, pressure perturbation has been calculated by using Lighthill's analogy. In Figure 5.13, pressure perturbation vs. time data has been shown. Currently, the data have been evaluated to handle statistical results. Then, the peaks have been obtained. After that, using FFT method, acoustic pressure vs. frequency has been obtained.

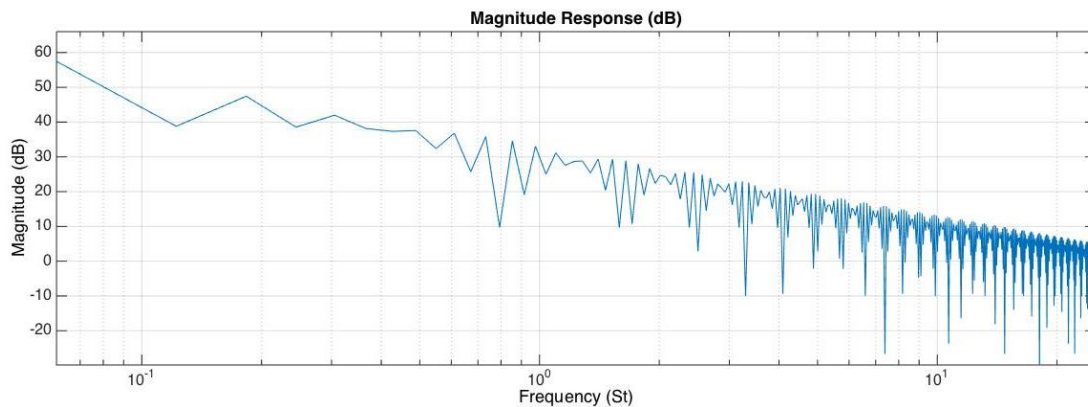


Figure 5.14 Acoustic magnitude response vs frequency in octave band

Result from FFT analysis; acoustic data have been obtained in the frequency domain. During the data handling, octave band filtering has been utilized to see acoustic data in detail. As mentioned before, at acoustic section, at high frequency region contains

shock broadband noise. As seen in Figure 5.15, at high frequency domain broadband shock noise is dominant.

(Seiner, 1984; Tam, 1995)

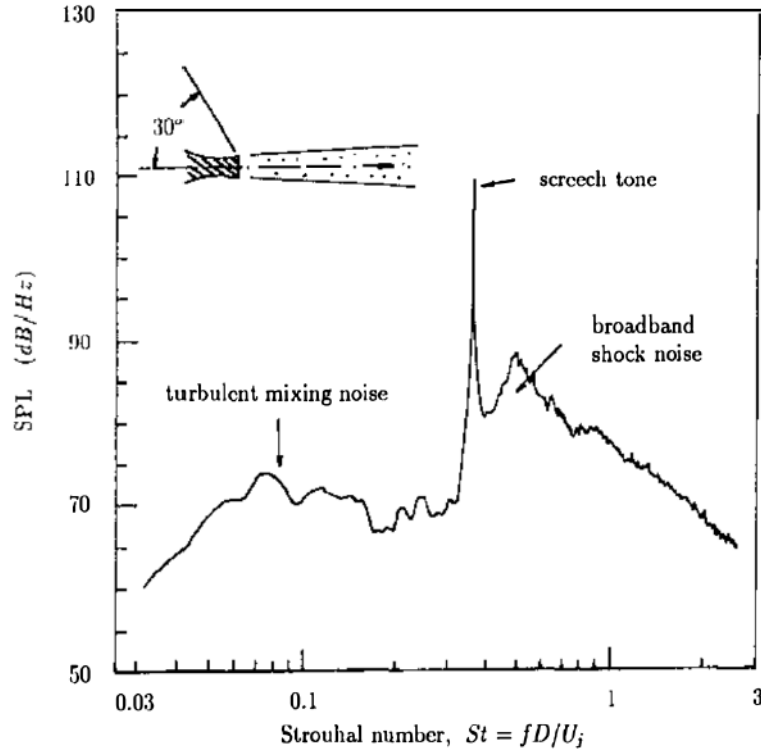


Figure 5.15 Jet noise contributions

In code structure, flow has been assumed as inviscid and non-turbulent. In other words, simulated jet flow does not contain any turbulent term. Due to that reason, by developed code, only shock-dominated section can be determined. The comparison of the literature and the result data demonstrate similar characteristic at high frequency domain. However, the low frequency domain is absolutely different. Also screech tone could not be derived in-house tool.

6. CONCLUSIONS AND RECOMMENDATIONS

In this study, numerical investigation of supersonic jet aerodynamic and aero acoustic assessment has been performed using fluid dynamics and acoustic principles and assumptions.

During the evaluations, in-house CFD code has been created. By using MATLAB programming language, code schemes have been developed. The code consists of three different sections. One of them regards grid generation and grid connectivity by working with ANSA tool as a couple. The total grid sequence has been created in ANSA and it has been modified by MATLAB to gather data efficiently. The second part of the code contains main function in other words LEE solver. And the final part consists of acoustic data handling and FFT analyze.

In grid generation section, ANSA commercial tool has generated fully quad elements. It's a requirement for the solver. The solver works only with quad element scheme. Generated grid has been formed to readable version. This operation has been performed by MATLAB tool. It's an important point, because understanding neighbor element definition is another requirement for the solver.

In solver scheme, Utilizing LEE approach, compressible supersonic flow was simulated as transient. Supersonic flow that has numerous complex discretizations has been modelled in detail in project scope. At different time step, different shock and flow structure has revealed. These are observed as clear as real life situation. In project scope, AUSM+ method that is a very efficient method for compressible flow has been utilized. This method works firmly with related problem or situation. As a conclusion, pressure, density and velocity data have been obtained in different time step. Each time step has been recorded in a folder to read during the post-process and acoustic analysis.

In the last section of the scheme, post process and pressure RMS outputs have been evaluated. This output gives information about acoustic source and propagation. From the outputs, noise magnitude distribution has been shown.

To confirm the result of in-house code, benchmark studies have been performed. Besides, acoustic data determination and acoustic energy calculation have been demonstrated in the last session.

From the study, acoustic analysis and aerodynamic analysis ability have been achieved. Created code can be applied to different geometries and cases. By using created numeric code, futuristic approaches and the calculation can be reformed.

Addition to this study, effects of turbulence eddy structure to acoustic noise determination can be evaluated. Turbulence effect can be obtained adding required terms to the developed solver scheme. Addition of 3rd dimensional terms, viscous terms and turbulence terms to solver scheme, future work can be performed perfectly.

In this project scope, only the first chapter of this futuristic work has been performed. The project has been accomplished by providing detailed aerodynamic and aero-acoustic assessment of the jet nozzle from numerical approach point of view.

REFERENCES

- Bridges, J.** (2012). Acoustic Measurements of Rectangular Nozzles with Bevel. *18th AIAA/CEAS Aeroacoustics Conference (33rd AIAA Aeroacoustics Conference)* (s. 226-235). AIAA.
- Bridges, J.** (2006). *Small Hot Jet Acoustic Rig Validation*. Cleveland: NASA.
- Courant, R., Friedrichs, K., & Lewy, H.** (1967). On the partial difference equations of mathematical physics. *IBM Journal of Research and Development* 11 (2) , 215–234.
- Curle, N.** (1955). The Influence of Solid Boundaries upon Aerodynamic Sound. *Proceedings of the Royal Society A: Mathematical, Physical and Engineering Sciences* 231 (1187) , 505-512.
- Daniel A. Russell, J. P.-J.** (1999). Acoustic monopoles, dipoles, and quadrupoles: An experiment revisited. *American Journal of Physics* 67 (8) , 660-664.
- Errede, S.** (2002). *The Human Ear – Hearing, Sound Intensity and Loudness Levels*. Illinois: UIUC Physics 406 Acoustical Physics of Music.
- Fluent Inc.** (2002). *User's Guide for FLUENT 6.0*.
- George, W. K.** (2005). *Lectures in Turbulence for the 21st Century*. Göteborg, Sweden: Department of Thermo and Fluid Engineering.
- Goldstein, M.** (2001). *Aeroacoustics*. New York: McGraw- Hill.
- Kirchhoff, G. R.** (1883). Zur Theorie der Lichtstrahlen,. *Annalen tier Physik und Chemie, Vol. 18* , 663-695.
- Lighthill, M. J.** (1952). On Sound Generated Aerodynamically. I. General Theory. *Proceedings of te Royal Society A: Mathematical, Physical and Engineering Sciences* 211 , 564-587.
- Lighthill, M. J.** (1954). On Sound Generated Aerodynamically. II. Turbulence as a Source of Sound. *Proceedings of the Royal Society A: Mathematical, Physical and Engineering Sciences* 222 (1148) , 1-31.
- Liou, M.-S.** (1996). A Sequel to AUSM: AUSM+. *JOURNAL OF COMPUTATIONAL PHYSICS* 129 , 364–382.

- Nyquist, H.** (2002). Certain topics in telegraph transmission theory. *Trans. AIEE*, vol. 47 , 617–644.
- Oengoeren, A. a.** (1998). A comprehensive study of vortex shedding, acoustic resonance and turbulent buffeting in normal triangular tube bundles. *Journal of Fluids and Structures*, Vol. 12 , 717-758.
- Randall, R.** (1987). *Frequency Analysis*. Glostrup, Denmark: Larsen & Son A/S.
- Seiner, J. M.** (1984). Advances in high speed jet aeroacoustics. *AIAA/NASA 9th Aeroacoustics Conference*. AIAA.
- Tanna, H. K.** (1977). An Experimental Study of Jet Noise Part II: Shock Associated Noise. *Journal of Sound and Vibration* 50(3), , 429-444.
- Toro, E. F.** (1999). *Riemann Solver and Numerical Methods for Fluid Dynamics*.
- White, F. M.** (2006). *Viscous Fluid Flow* ((3rd. ed.) b.). New York: McGraw-Hill.
- Williams, J. E., & Hawkings, D. L.** (1969). Sound Generation by Turbulence and Surfaces in Arbitrary Motion. *Philosophical Transactions of the Royal Society A: Mathematical, Physical and Engineering Sciences* 264 (1151) , 321-342.

APPENDICES

APPENDIX A:

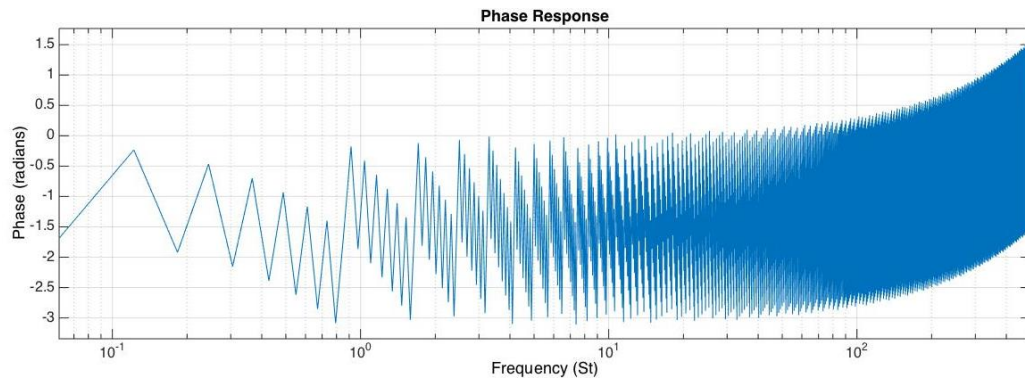


Figure A.0.1 : Phases vs frequency

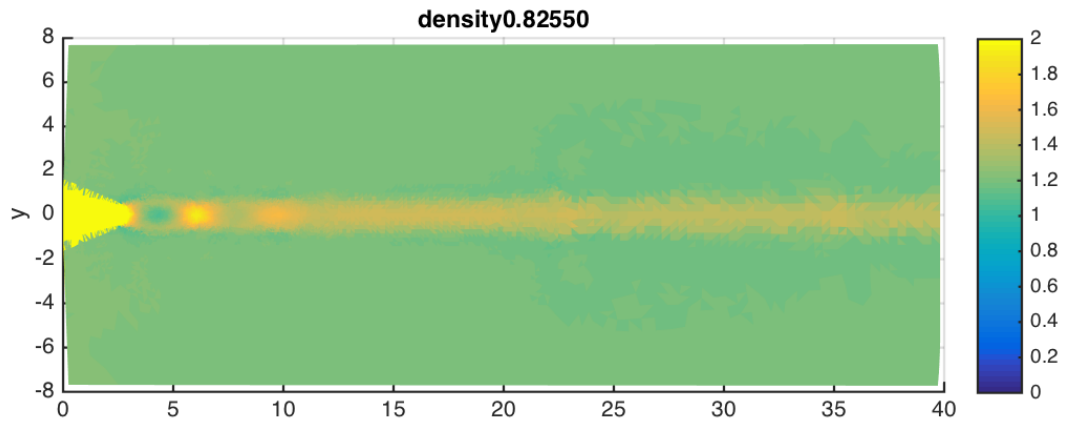
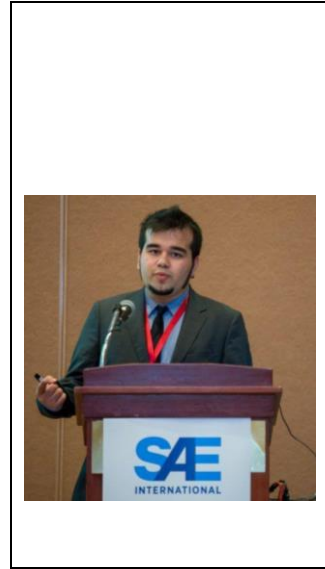


Figure A.0.2 : Density distribution on domain for $t=0.82550$

CURRICULUM VITAE



Name Surname: Ramiz Ömür İçke

Place and Date of Birth: Sivas -24/07/1989

E-Mail: eromir@gmail.com/icker@itu.edu.tr/oicke@ford.com

EDUCATION:

B.Sc.: ITU, Aeronautical Engineering (2011)

ITU, Astronautical Engineering (2011)

PROFESSIONAL EXPERIENCE AND REWARDS:

- Ford Otosan, Aerodynamic Development Engineer (2012-....)

PUBLICATIONS, PRESENTATIONS AND PATENTS ON THE THESIS: